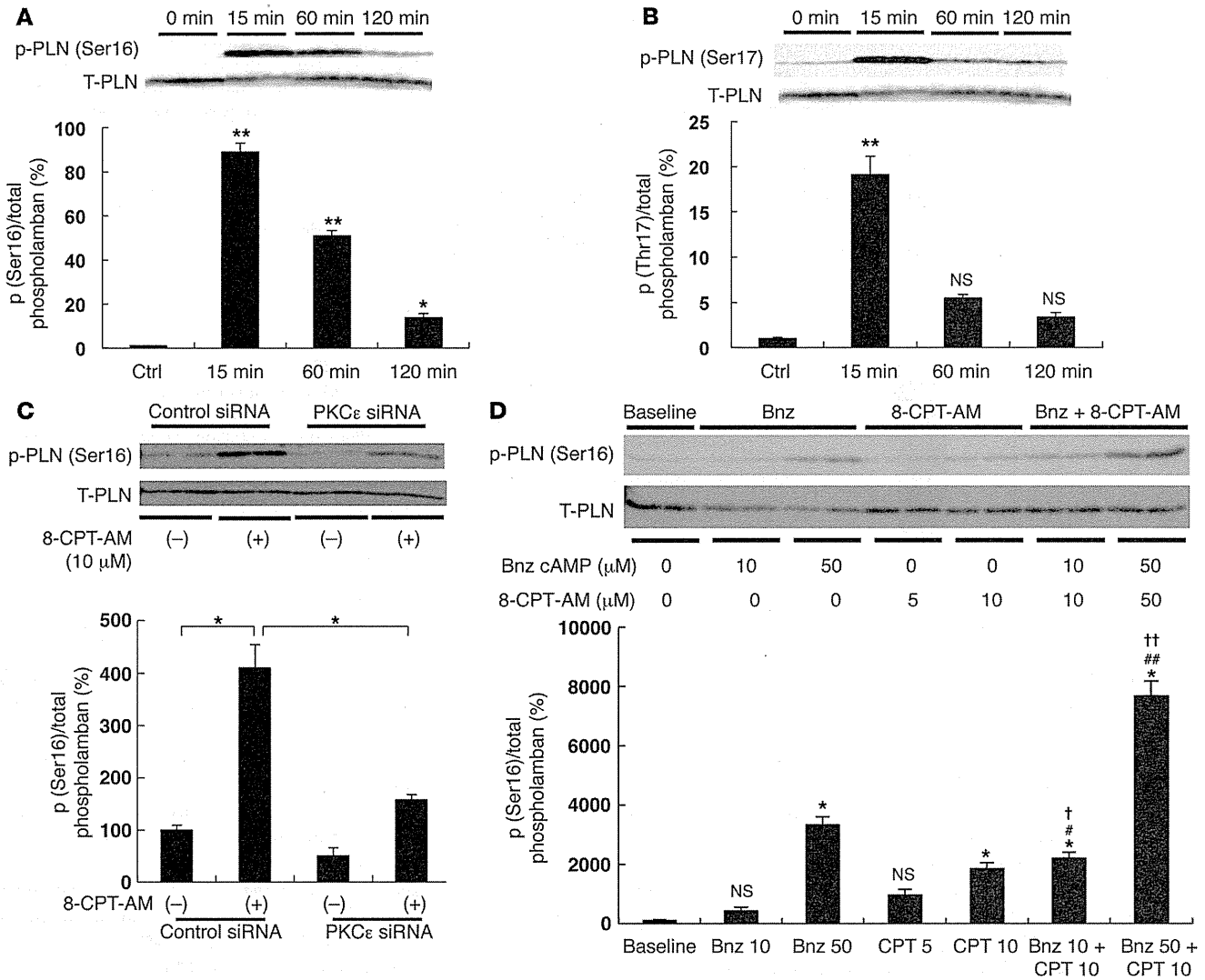

Figure 2

Effects of EPAC activation on PLN phosphorylation in neonatal rat cardiac myocytes. (**A** and **B**) Treatment of neonatal rat cardiac myocytes with 8-CPT-AM (10 μM). PLN phosphorylation on serine-16 was significantly increased at 15 minutes and remained significantly (*$P < 0.05$ or **$P < 0.01$ versus 0 minutes, $n = 4$) greater at 120 minutes than at 0 minutes (**A**). PLN phosphorylation on threonine-17 was also significantly increased at 15 minutes after treatment. However, increase fell below significance at 60 minutes versus 0 minutes and remained unchanged at 120 minutes (P = NS, versus 0 minutes, $n = 4$) (**B**). Ratio of phosphorylated/total protein expression of PLN at baseline (0 min: Ctrl) was taken as 1-fold. (**C**) EPAC-mediated PLN phosphorylation on serine-16 was examined in neonatal rat cardiac myocytes transfected with PKCε siRNA or control siRNA (*$P < 0.01$, $n = 5$–7). Ratio of phosphorylated/total protein expression of PLN in cells transfected with control siRNA at baseline was taken as 100%. (**D**) PLN phosphorylation on serine-16 was examined in cells treated with Bnz-cAMP (50 μM) and/or 8-CPT-AM (10 μM). (##$P < 0.001$ versus Bnz-cAMP [50 μM] alone; ††$P < 0.001$ versus 8-CPT-AM [10 μM] alone). A similar tendency was observed when 10 μM Bnz-cAMP and 5 μM 8-CPT-AM were used together (#$P < 0.001$ versus Bnz-cAMP [10 μM] alone; †$P < 0.001$ versus 8-CPT-AM [5 μM] alone, $n = 4$–8; *$P < 0.01$ versus baseline, $n = 4$–8). Ratio of phosphorylated/total protein expression of PLN at baseline was taken as 100%.

PKC isoform with siRNA on PLN phosphorylation (Supplemental Figure 7A). Silencing of PKCα, PKCβ, PKCγ, and PKCδ did not affect the EPAC-mediated PLN phosphorylation on serine-16 with 8-CPT-AM (Supplemental Figure 8). However, when PKCε was silenced with siRNA (its specificity was confirmed: Supplemental Figure 7B), EPAC-mediated PLN phosphorylation on serine-16 was significantly attenuated compared with the control (control siRNA versus PKCε siRNA: 410% ± 44% versus 158% ± 10%, $n = 5$–7, $P < 0.01$), suggesting that PKCε plays a role in PLN phosphorylation on serine-16 by EPAC (Figure 2C).

EPAC phosphorylates PLN in an additive and independent manner with respect to PKA. In order to compare the roles of EPAC and PKA in PLN phosphorylation, we examined the effects of N^6-benzoyladenosine-cAMP (Bnz-cAMP), a PKA-selective cAMP analogue, and 8-CPT-AM, an EPAC-selective analogue (Figure 2D). The degree of PLN phosphorylation achieved with 8-CPT-AM (10 μM) was approximately 60% of that achieved with Bnz-cAMP (50 μM) (Bnz-cAMP versus 8-CPT-AM: 3324% ± 289% versus 1851% ± 202%, $n = 4$–8, $P < 0.001$). However, when 8-CPT-AM and Bnz-cAMP were used together, PLN phosphorylation was additively and significantly increased

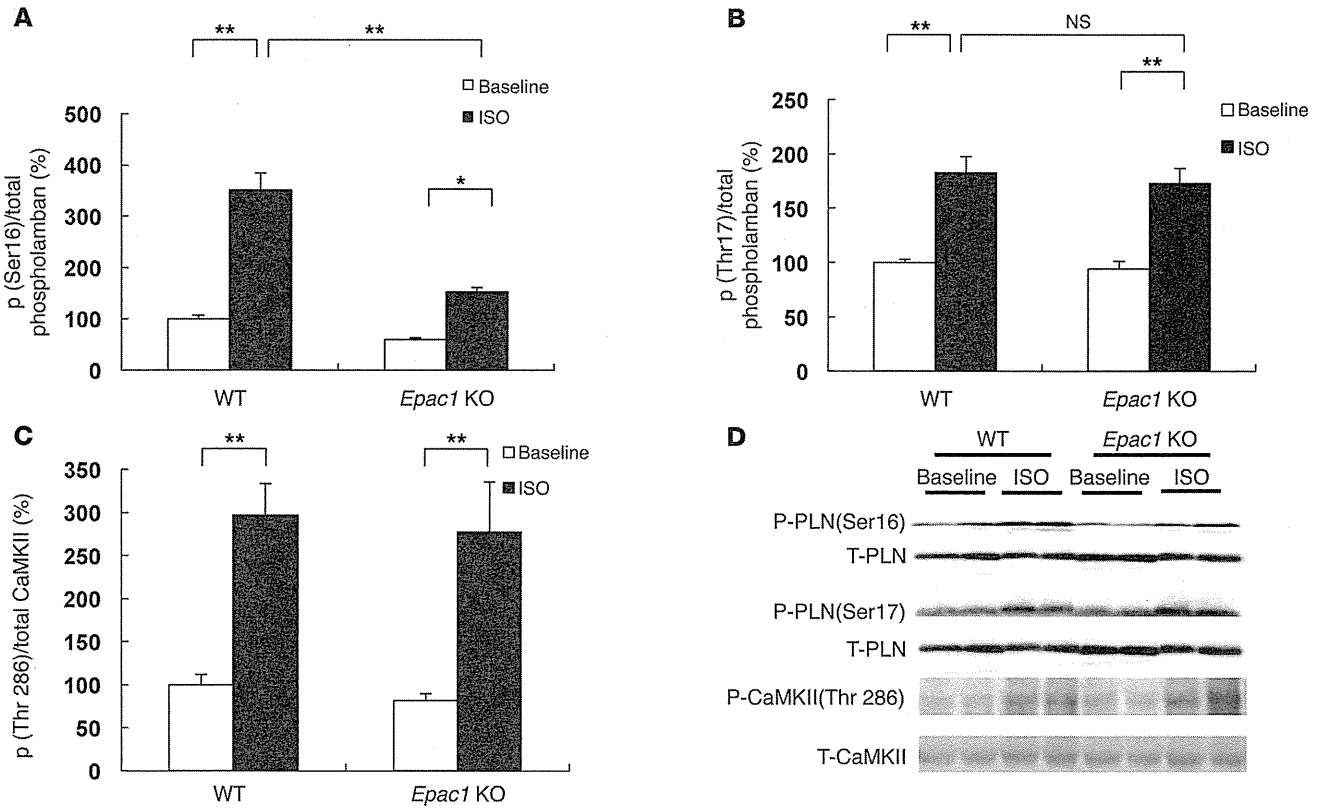

Figure 3

PLN phosphorylation on serine-16 and threonine-17 and CaMKII phosphorylation on threonine-286 in isolated WT or *Epac1* KO heart perfused according to Langendorf method with or without subsequent ISO (0.1 μM) for 5 minutes. (**A**) PLN phosphorylation on serine-16 was significantly increased (*$P < 0.05$, **$P < 0.01$) in response to ISO in WT and *Epac1* KO (WT: from 100% ± 7.0% to 351% ± 32%, $n = 6–8$; *Epac1* KO: from 60 ± 2.6 to 153% ± 9%, $n = 5$), but increase was significantly smaller in *Epac1* KO (153% ± 9%) compared with WT (351% ± 32%, **$P < 0.01$, $n = 5–6$). Ratio of phosphorylated/total protein expression of PLN in WT at baseline was taken as 100%. (**B**) PLN phosphorylation on threonine-17 was similar in WT and *Epac1* KO at baseline and was significantly increased in response to ISO in WT (from 100% ± 2.3% to 183% ± 14%, **$P < 0.01$, $n = 6–8$) and *Epac1* KO (from 94% ± 6.7% to 173% ± 13%, **$P < 0.01$, $n = 6–8$). Magnitudes of the increase were similar (P = NS). Ratio of phosphorylated/total protein expression of PLN in WT at baseline was taken as 100%. (**C**) CaMKII phosphorylation on threonine-286 was similar in WT and *Epac1* KO at baseline and was significantly increased (**$P < 0.01$) in response to ISO in WT (from 100% ± 12% to 297% ± 37%, $n = 5$) and *Epac1* KO (from 82% ± 7.7% to 278% ± 58%, $n = 5$). Magnitudes of increase were similar (P = NS). Ratio of phosphorylated/total protein expression of CaMKII in WT at baseline was taken as 100%. (**D**) Representative immunoblotting results of phosphorylation of PLN on serine-16 (upper) and threonine-17 (middle) and CaMKII on threonine-286 (lower). p-CaMKII, phosphorylated CaMKII; T-CaMKII, total CaMKII.

(7688% ± 497%) relative to that with Bnz-cAMP alone (3324% ± 289%) or with 8-CPT-AM alone (1851% ± 202%) ($P < 0.001$ versus Bnz-cAMP or 8-CPT-AM alone). A similar tendency was observed when 5 μM 8-CPT-AM and 10 μM Bnz-cAMP were used together, suggesting that EPAC-mediated PLN phosphorylation may be independent of PKA-mediated PLN phosphorylation. Taken together, these results indicate that PLN phosphorylation via EPAC is additive to that via PKA, and both EPAC and PKA might be required for maximal PLN activation via phosphorylation on serine-16.

Effects of infection with Ad-PKI-GFP on PLN phosphorylation in neonatal cardiac myocytes transfected with negative or EPAC1 siRNA. In order to confirm the role of EPAC1 in PKA-independent PLN phosphorylation, we generated recombinant adenovirus of mouse protein kinase inhibitor α-GFP (*Pkia*-GFP) infusion gene (Ad-PKI-GFP) and adenovirus of GFP (Ad-GFP) as controls and examined the effects of Ad-PKI-GFP infection on PLN phosphorylation in neonatal rat cardiac myocytes transfected with control or EPAC1 siRNA (Supplemental Figure 9A, Supplemental Figure 10, and ref. 44).

We first confirmed that more than 98% of cells appeared green and that GFP fluorescence was evenly distributed in the cytoplasm of cardiomyocytes infected with Ad-PKI-GFP or Ad-PKI at MOI 100 (Supplemental Figure 10B).

We next performed Western blotting and found that PLN phosphorylation on serine-16 was significantly increased in cells infected with Ad-GFP or Ad-PKI-GFP in addition to control siRNA transfection after ISO treatment (10 μM) for 15 minutes. However, the magnitude of the increase was significantly smaller in cells transfected with Ad-PKI-GFP than with Ad-GFP (Ad-GFP [lane 2] versus Ad-PKI-GFP [lane 4]: 60 ± 2.6 versus 45 ± 3.1-fold, $P < 0.05$, $n = 4$) (Supplemental Figure 10C). In order to examine the role of EPAC1 in PKA-independent PLN phosphorylation on serine-16, we examined the effect of EPAC1 siRNA transfection and found that silencing EPAC1 significantly decreased the ISO-promoted PLN phosphorylation on serine-16 in cells infected with Ad-PKI-GFP (lane 5: 22 ± 0.6-fold, $P < 0.01$, $n = 4$). However, pretreatment with KN-93 (10 μM for 30 minutes), a specific CaMKII inhibitor,

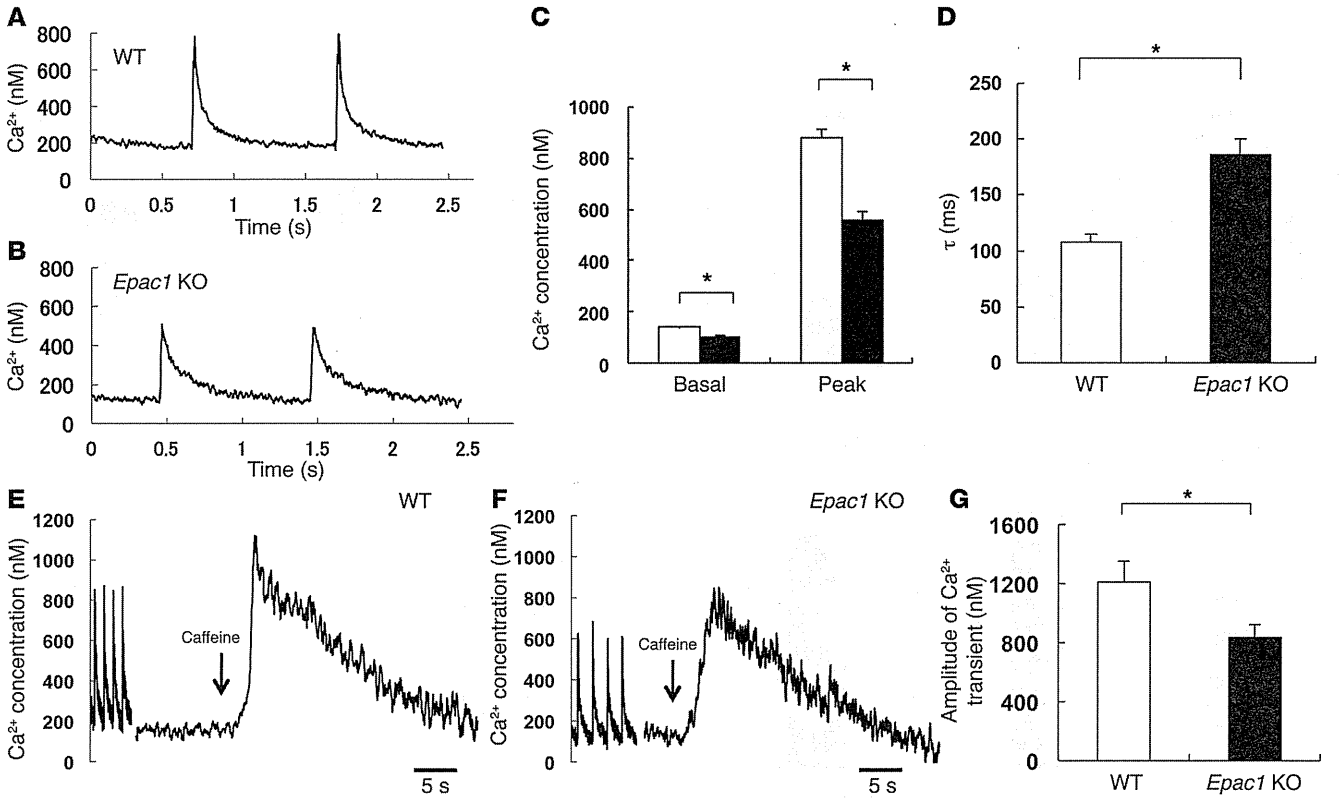

Figure 4

Ca^{2+} transient of adult isolated cardiac myocytes from *Epac1* KO. (**A** and **B**) Typical recordings of Ca^{2+} transients in cardiac myocytes from WT (**A**) and *Epac1* KO (**B**). Note that the basal and peak Ca^{2+} transient amplitude and decay rate are smaller in *Epac1* KO (n = 32 cells from 4 animals each). (**C** and **D**) Ca^{2+} transient parameters of isolated cardiac myocytes from *Epac1* KO and WT. The basal Ca^{2+} concentration (WT versus *Epac1* KO: 139 ± 6.8 versus 99 ± 11.8 nM) and peak Ca^{2+} concentration (WT versus *Epac1* KO: 883 ± 35.3 versus 559 ± 33.2 nM) were significantly lower in *Epac1* KO than in WT (**C**). The decay time constant (τ) was significantly larger in *Epac1* KO than in WT (WT versus *Epac1* KO: 108 ± 6.6 versus 187 ± 13.2 ms) (n = 32 cells, $^*P < 0.05$) (**D**). (**E** and **F**) Typical recordings of Ca^{2+} transients after caffeine (10 mM) treatment of cardiac myocytes from WT (**E**) and *Epac1* KO (**F**). (**G**) Peak Ca^{2+} concentration after caffeine (10 mM) treatment was significantly decreased in *Epac1* KO compared with WT (WT versus *Epac1* KO: 1210 ± 143 versus 835 ± 87.6 nM, n = 7, $^*P < 0.05$).

did not decrease ISO-promoted PLN phosphorylation on serine-16 in cells transfected with control siRNA (lane 6: 37 ± 3.1-fold, P = NS, n = 8) (Supplemental Figure 10C).

We also examined whether PLN phosphorylation on threonine-17 was increased in cells transfected with Ad-GFP or Ad-PKI-GFP in addition to control siRNA after ISO treatment (10 μM) for 15 minutes. However, the magnitudes of the increase were similar in both cases (Ad-GFP [lane 2] versus Ad-PKI-GFP [lane 4]: 59 ± 0.04 versus 56 ± 0.05-fold, P = NS, n = 8) (Supplemental Figure 10D). Transfection of EPAC1 siRNA significantly decreased ISO-promoted PLN phosphorylation on threonine-17 in cells transfected with Ad-PKI-GFP (lane 5: 41 ± 0.04, $P < 0.05$, n = 8) as in the case of serine-16. However, KN-93 pretreatment (10 μM for 30 minutes) abrogated the ISO-promoted PLN phosphorylation on serine-17 in cells transfected with control siRNA (lane 6: 1.4 ± 0.003, $P < 0.01$, n = 8) (Supplemental Figure 10D).

Together with the data in Figure 2D, these data obtained with Ad-PKI-GFP clearly demonstrated that EPAC1 and PKA regulate PLN phosphorylation on serine-16 in an additive and an independent manner. Also, EPAC1 regulates PLN phosphorylation at both serine-16 and threonine-17 in vitro, in addition to PKA and CaMKII.

The increase of PLN phosphorylation on serine-16 with ISO was decreased in Epac1 KO. We next examined the phosphorylation of PLN in total homogenate prepared from WT and *Epac1* KO hearts perfused with the Langendorf method. Hearts were perfused with Krebs solution at constant pressure with or without the treatment of ISO (0.1 μM) for 5 minutes (45), then rapidly frozen in liquid nitrogen for Western blotting (Figure 3).

PLN phosphorylation on serine-16 was significantly decreased in *Epac1* KO compared with that in WT at baseline (WT versus *Epac1* KO: 100% ± 7.0% versus 60% ± 2.5%, $P < 0.05$, n = 5–8). It was significantly increased in response to ISO, but the magnitude of the increase was significantly smaller in *Epac1* KO (WT versus *Epac1* KO: 351% ± 32% versus 153% ± 9%, n = 5–6, $P < 0.01$) (Figure 3A). PLN phosphorylation on threonine-17 was similar in both WT and *Epac1* KO at baseline (100% ± 3.0% versus 94% ± 6.7%, n = 8, P = NS). However, it was significantly increased in both WT and *Epac1* KO in response to ISO ($P < 0.01$), and the magnitudes of the increase were similar (WT versus *Epac1* KO: 183% ± 14% versus 173% ± 13%, n = 6, P = NS) (Figure 3B). CaMKII phosphorylation on threonine-286 was also similar in WT and *Epac1* KO at baseline (WT versus *Epac1*: 100% ± 12% versus 82% ± 7.7%, n = 5, P = NS). It was significantly increased in both WT and *Epac1* KO in response

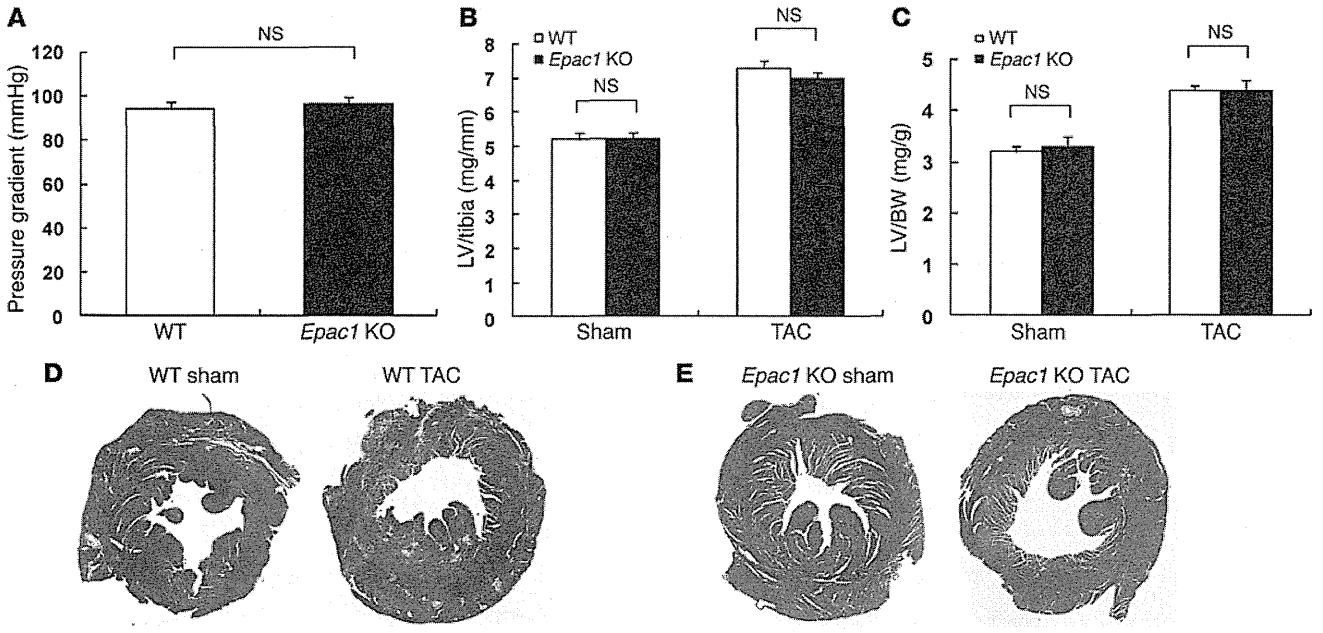

Figure 5

Comparison of cardiac hypertrophy after aortic banding (TAC) in WT and *Epac1* KO. (**A**) Pressure gradients were not different in WT and *Epac1* KO at 3 weeks after TAC (n = 13-16, P = NS). (**B** and **C**) LV weight (mg)/tibial length (mm) ratio (**B**) and LV weight (mg)/body weight (BW, g) ratio (**C**) were determined at 3 weeks. The degree of cardiac hypertrophy was increased at 3 weeks, but was similar in WT and *Epac1* KO (LV/tibial length ratio for WT versus *Epac1* KO: 7.3 ± 0.2 versus 7.0 ± 0.2; LV/BW ratio for WT versus *Epac1* KO: 4.4 ± 0.1 versus 4.4 ± 0.2, n = 18–20, P = NS). (**D** and **E**) Representative gross LV section of Masson-trichrome staining in sham-operated and TAC-operated WT and *Epac1* KO heart. Note that the degree of cardiac hypertrophy was similar, but the fibrotic area after aortic banding was smaller in *Epac1* KO than that in WT.

to ISO (P < 0.01), and the magnitudes of the increase were similar (WT versus *Epac1* KO: 297% ± 37% versus 278% ± 58%, n = 5, P = NS) (Figure 3C). These data indicate that PLN phosphorylation on serine-16, the major site of PKA-mediated phosphorylation, is also regulated by EPAC1. However, EPAC1 does not alter PLN phosphorylation on threonine-17, the major site of CaMKII-mediated phosphorylation, at baseline or in response to ISO.

Silencing EPAC1 in cardiac myocytes attenuates ISO-mediated increases of RyR2 phosphorylations on serine-2808 and serine-2814. PKA and CaMKII-mediated phosphorylation of RyR2 play important roles in modulating cardiac contractility and arrhythmogenesis. It was reported that RyR2 phosphorylation on serine-2808 is mediated by PKA, while RyR2 phosphorylation on serine-2814 is mediated by CaMKII (46). More recently, both sites have been reported to be phosphorylated by PKA and CaMKII, and their phosphorylation is required for adequate RyR2 functional activity (11). We thus examined ISO-induced (10 μM for 3 minutes) phosphorylation on serine-2808 and serine-2814 of RyR2 in neonatal rat cardiac myocytes transfected with control or EPAC1 siRNA because we found that phosphorylated and total RyR2 antibodies did not work well in cardiac homogenate prepared from mouse heart perfused with the Langendorf method (Supplemental Figure 9A and Supplemental Figure 11). RyR2 phosphorylation levels on serine-2808 and serine-2814 were similar in cells transfected with control or EPAC1 siRNA at baseline (serine-2808: control siRNA versus EPAC1 siRNA: 100% ± 1.9% versus 130% ± 4.9%, n = 4, P = NS; serine-2814: control siRNA versus EPAC1 siRNA: 100% ± 16% versus 116% ± 16%, n = 4–6, P = NS). They were significantly increased in response to ISO, but the magnitudes of the increase on both serine-2808 (Supplemental Figure 11B) and serine-2814 (Supplemental Figure 11C) were significantly smaller in cells transfected with EPAC1 siRNA than those in cells transfected with control siRNA (serine-2808: control siRNA versus EPAC1 siRNA 268% ± 8.3% versus 199% ± 13%; P < 0.01, n = 6; serine-2814: control siRNA versus EPAC1 siRNA 220% ± 13% versus 170% ± 2.3%, P < 0.05, n = 4–6). These data indicate that EPAC1 regulates RyR2 phosphorylation on serine-2808 and serine-2814 in addition to PKA and CaMKII.

Intracellular Ca^{2+} concentration is decreased in Epac1 KO myocytes. Cardiac contraction and relaxation are influenced by the intracellular increase in Ca^{2+} during systole and its decrease during diastole. Sarcoplasmic reticulum Ca^{2+} uptake is regulated via PLN phosphorylation. PLN phosphorylation has recently been concluded to play a prominent role in the regulation of myocardial contraction as well as relaxation based on findings in *Pln* knockout mice (12).

We thus examined the intracellular Ca^{2+} concentration in isolated cardiac myocytes of *Epac1* KO (Figure 4, A and B). The basal and peak Ca^{2+} concentrations were significantly decreased in *Epac1* KO compared with WT (basal Ca^{2+} in WT versus *Epac1* KO 139 ± 6.8 versus 99 ± 11.8 nM, n = 32, P < 0.01; peak Ca^{2+} in WT versus *Epac1* KO: 883 ± 35.3 versus 559 ± 33.2 nM, n = 32, P < 0.01) (Figure 4C). The decay time constant (τ) was significantly larger in *Epac1* KO than that in WT controls (WT versus *Epac1* KO: 108 ± 6.6 versus 187 ± 13.2 ms, n = 32, P < 0.01) (Figure 4D). We also examined the cytoplasmic Ca^{2+} concentration after addition of caffeine (10 mM) as a measure of Ca^{2+} content in SR in isolated cardiac myocytes of WT and *Epac1* KO (Figure 4, E–G). The amplitude of the caffeine-induced increase in cytoplasmic Ca^{2+} concentration was significant in WT compared with *Epac1*

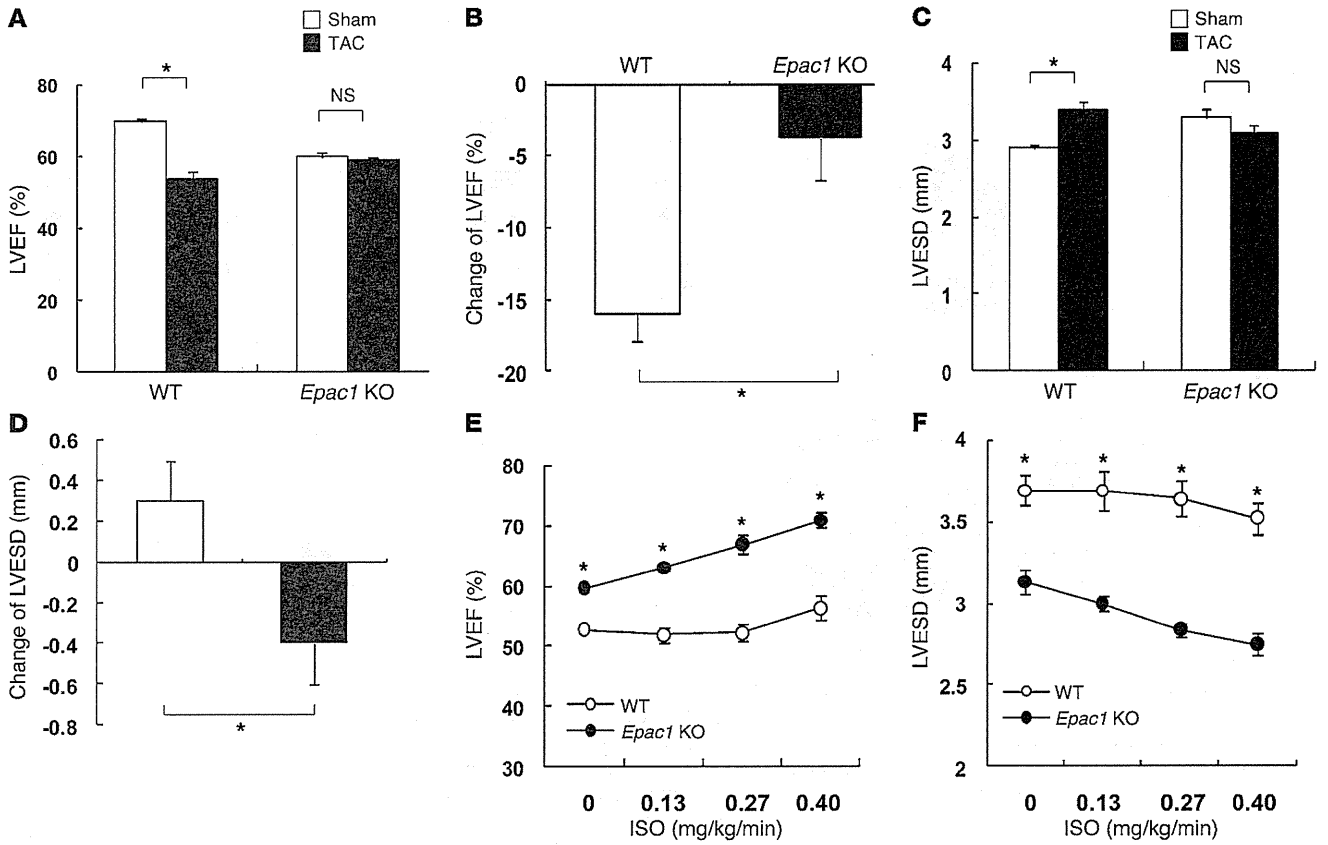

Figure 6

Changes in LV function at 3 weeks after aortic banding (TAC) in WT and *Epac1* KO. Echocardiographic measurements of LV function were performed at 3 weeks after TAC of WT and *Epac1* KO and in sham-operated controls. (**A** and **B**) LVEF was significantly decreased in WT (*$P < 0.01$), but not in *Epac1* KO (P = NS) at 3 weeks (WT versus *Epac1* KO: from 70% ± 0.8% to 54% ± 2.0% versus from 60% ± 1.1% to 59% ± 0.7%, n = 17–30) (**A**). The data were compared with those from sham-operated controls at 3 weeks in each mouse. Change of LVEF from sham-operated controls at 3 weeks after TAC was significantly greater in WT than that in *Epac1* KO (**B**) (n = 17–31, *$P < 0.01$). (**C** and **D**) LVESD was significantly increased in WT, but not in *Epac1* KO at 3 weeks after TAC (**C**). The data were compared with those from sham-operated controls at 3 weeks. Change of LVESD from sham-operated controls at 3 weeks after banding was greater in WT than that in *Epac1* KO (n = 17–31, *$P < 0.01$) (**D**). The decrease of LVESD in response to intravenous acute ISO infusion (0, 0.13, 0.27, 0.40 mg/kg/min for 5 minutes) was depressed in WT, but not in *Epac1* KO (n = 4–5, *$P < 0.01$). (**E** and **F**) The increase of LVEF (**E**) and the decrease of LVESD (**F**) in response to intravenous acute ISO infusion (0, 0.13, 0.27, 0.40 mg/kg/min for 5 minutes) were depressed in WT, but not in *Epac1* KO (n = 4–5, *$P < 0.01$) (**E**).

KO (WT versus *Epac1* KO: 1210 ± 143 versus 835 ± 87.6 nM, n = 7, $P < 0.05$), indicating that the Ca^{2+} content in SR was decreased in *Epac1* KO compared with WT.

Activities of L-type Ca^{2+} channel and NCX channel in Epac1 KO are similar to those in WT. We measured the L-type Ca^{2+} channel current (I_{CaL}) and Na^{+}-Ca^{2+} exchange current (I_{NCX}) using the cell patch-clamp technique in isolated cardiac myocytes of *Epac1* KO and confirmed that the density and current-voltage relationships of I_{CaL} (Supplemental Figure 12) and I_{NCX} (Supplemental Figure 13) were not different. We also examined the response of I_{CaL}, a PKA-dependent target, in response to ISO (10^{-7} M) and confirmed that it was not different between WT and *Epac1* KO (Supplemental Figure 12B and ref. 6).

Disruption of EPAC1 does not affect development of cardiac hypertrophy, but prevents heart failure in pressure overload stress. In order to examine the role of EPAC1 in the development of heart failure, we performed aortic banding in *Epac1* KO and WT for 3 weeks. The pressure gradients were similar in WT and *Epac1* KO at 3 weeks after banding (Figure 5A). At baseline, there was no difference between WT and *Epac1* KO in the LV weight (mg)/tibial length (mm) (LV/tibial length ratio in WT versus *Epac1* KO: 5.2 ± 0.2 versus 5.2 ± 0.2 mg/mm, n = 18–20, P = NS). The degree of cardiac hypertrophy was increased at 3 weeks, but remained similar in *Epac1* KO and WT (LV/tibial length ratio in WT versus *Epac1* KO: 7.3 ± 0.2 versus 7.0 ± 0.2, n = 18–20, P = NS) (Figure 5, B, D, and E). The change of LV/body weight ratio, another index of cardiac hypertrophy, confirmed the finding based on LV/tibial length ratio (WT versus *Epac1* KO: from 3.2 ± 0.1 to 4.4 ± 0.1 versus from 3.3 ± 0.2 to 4.4 ± 0.2 mg/g, n = 18–20, P = NS) (Figure 5C).

At 3 weeks after banding, however, cardiac function (LVEF) was significantly decreased in WT ($P < 0.01$), while it remained unchanged in *Epac1* KO (WT versus *Epac1* KO: from 70% ± 0.8% to 54% ± 2.0% versus from 60% ± 1.1% to 60% ± 0.7%, n = 17–30) (Figure 6, A and B). LVESD was increased significantly in WT at 3 weeks after banding ($P < 0.01$), while it remained unchanged in *Epac1* KO (WT versus *Epac1* KO: from 2.9 ± 0.04 to 3.3 ± 0.1 versus from 3.4 ± 0.1 to 3.1 ± 0.1 mm, n = 17–31) (Figure 6, C and D). Hemodynamic measurements demonstrated that Max dP/dt was significantly decreased in WT, but not in *Epac1*

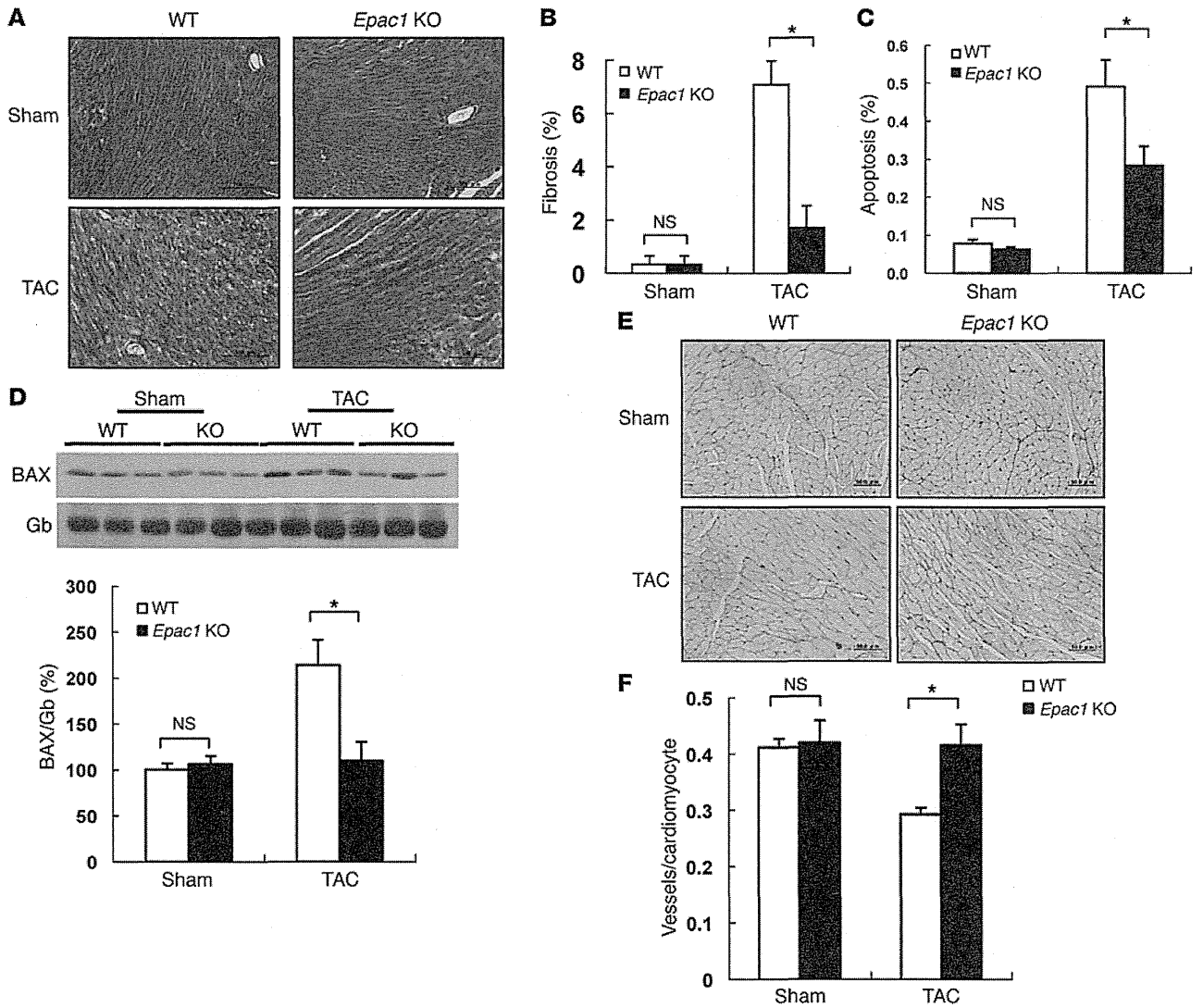

Figure 7

Accelerated morphological deterioration after aortic banding (TAC) was attenuated in *Epac1* KO. (**A**) Representative images of Masson-trichrome–stained sections of sham-operated and TAC-operated heart of WT and *Epac1* KO at 3 weeks. Scale bars: 100 μm. (**B**) Quantitative analysis of the fibrotic area in sham-operated and TAC-operated heart at 3 weeks after TAC of WT and *Epac1* KO. Cardiac fibrosis was significantly increased after TAC in WT and *Epac1* KO, but magnitude of the increase was much smaller in *Epac1* KO ($n = 4$, $^*P < 0.01$). (**C**) TUNEL-positive myocytes in LV myocardium were counted in WT and *Epac1* KO and expressed as percentage of total myocytes. Number of TUNEL-positive myocytes was significantly smaller in *Epac1* KO than in WT at 3 weeks after aortic banding ($n = 4$–6, $^*P < 0.05$). (**D**) Expression of BAX protein was compared between WT and *Epac1* KO. Protein expression of BAX was determined by Western blot analysis, which showed greater expression in WT than in *Epac1* KO at 3 weeks after TAC ($n = 4$, $^*P < 0.05$). Expression of BAX protein in the heart of sham-operated control WT was taken as 100%. Representative immunoblotting results are shown. (**E**) Representative images of double-immunostaining for dystrophin (brown) and PECAM (blue) of WT and *Epac1* KO at baseline and 3 weeks after aortic banding. Scale bars: 50 μm. (**F**) Number of microvessels per cardiomyocyte was compared in WT and *Epac1* KO at baseline and at 3 weeks after aortic banding ($n = 4$, $^*P < 0.01$).

KO (WT versus *Epac1* KO: from 9091 ± 240 to 6359 ± 393 mmHg [$P < 0.01$] versus from 7246 ± 226 to 6811 ± 250 mmHg, $n = 13$–17) and the magnitude of the decrease was much smaller in *Epac1* KO (Supplemental Figure 14, A and D). Min dP/dt was significantly increased in WT, while it remained unchanged in *Epac1* KO (WT versus *Epac1* KO: from −9110 ± 240 to −4389 ± 469 versus from −6201 ± 125 to −5131 ± 334 mmHg, $n = 13$–18, P = NS) and the magnitude of the increase was much smaller in *Epac1* KO (Supplemental Figure 14, B and E). End-diastolic pressure (EDP) was significantly increased in both WT and *Epac1* KO (WT versus *Epac1* KO: from 7.2 ± 0.3 to 16.8 ± 1.4 versus from 6.8 ± 0.3 to 11.5 ± 1.1 mmHg, $n = 13$–22, $P < 0.01$), but the magnitude of the increase was significantly smaller in *Epac1* KO (Supplemental Figure 14, C and F).

We also examined the effect of long-term chronic pressure overload on cardiac hypertrophy and cardiac function at 5 weeks after banding in *Epac1* KO (Supplemental Figure 15A). At 5 weeks after banding, cardiac hypertrophy was increased in both WT and *Epac1* KO and the magnitude of the increase was similar (WT versus *Epac1*

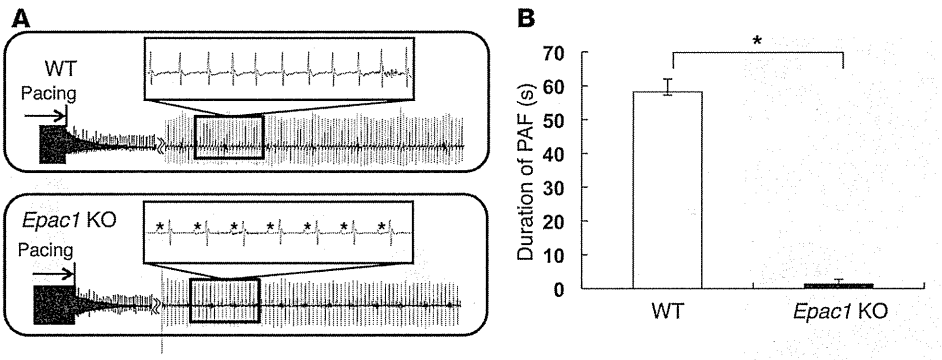

Figure 8

The duration of AF induced by transesophageal rapid atrial pacing was decreased in *Epac1* KO. (**A** and **B**) Transesophageal pacing was performed at a cycle length of 30 ms for 1 minute, and the duration of pacing-induced AF was examined in *Epac1* KO and WT (**A**). The duration of AF was significantly decreased in *Epac1* KO compared with WT controls. AF was induced in all WT mice and its duration was 59 ± 3.4 seconds (n = 4). In *Epac1* KO, we found that AF was hardly inducible (1.4 ± 1.0 seconds, n = 5, $^{**}P < 0.01$ versus WT) (**B**).

KO, LV/tibia length ratio: 7.7 ± 0.4 versus 7.7 ± 0.2 mg/mm; LV/body weight ratio: 4.4 ± 0.3 versus 4.6 ± 0.2 mg/g, n = 15, P = NS) (Supplemental Figure 15, B and C). However, cardiac function was significantly decreased in WT ($P < 0.01$), while it remained unchanged in *Epac1* KO (from 60% ± 1.1% to 61% ± 0.7%, n = 15). LVESD was increased significantly in WT at 5 weeks after banding ($P < 0.01$), while it remained unchanged in *Epac1* KO (WT versus *Epac1* KO: from 2.9 ± 0.04 to 3.3 ± 0.1 versus from 3.3 ± 0.1 to 3.2 ± 0.1 mm, n = 15–31) (Supplemental Figure 15, D–F). These results indicate that *Epac1* KO developed hypertrophy similar to that of WT in response to pressure overload, but did not develop cardiac failure.

Cardiac fibrosis and apoptosis are attenuated in Epac1 KO. There was no difference in degree of fibrosis between WT and *Epac1* KO at baseline. Thus, the development of cardiac fibrosis was unaffected in *Epac1* KO (WT versus *Epac1* KO: 0.3% ± 0.09% versus 0.3% ± 0.06%, n = 5, P = NS). Aortic banding increased the area of fibrosis in both WT and *Epac1* KO (Figure 5, D and E), but the magnitudes of increase were much smaller in *Epac1* KO (WT versus *Epac1* KO: 7.1% ± 0.9% versus 1.7% ± 0.8%, n = 4, $P < 0.01$) (Figure 7, A and B).

Similarly, there was no difference in the number of TUNEL-positive cells between WT and *Epac1* KO at baseline (WT versus *Epac1* KO: 0.08% ± 0.01% versus 0.06% ± 0.007%, n = 6, P = NS). Aortic banding increased the number of TUNEL-positive cells in both WT and *Epac1* KO, but the magnitudes of increase were much smaller in *Epac1* KO (WT versus *Epac1* KO: 0.49% ± 0.07% versus 0.24% ± 0.05%, n = 4–6, $P < 0.05$) (Figure 7C). To examine changes in the molecules involved in apoptosis signaling, we quantitated BAX protein, an accelerator of apoptosis (31), in WT and *Epac1* KO and found that its expression after banding was significantly increased, by 2.1-fold in WT, but not in *Epac1* KO (n = 4–6, $P < 0.05$) (Figure 7D).

Myocardial blood flow is preserved in Epac1 KO. We next examined cardiac response to intravenous ISO infusion, which is a hallmark of transmural myocardial blood flow, at 3 weeks after aortic banding (47). The increase of LVEF and decrease of LVESD in response to ISO were blunted in WT, but they were preserved in *Epac1* KO (n = 4–5, $P < 0.01$ versus WT), suggesting that cardiac angiogenesis during aortic banding might be preserved in *Epac1* KO (Figure 6, E and F, and ref. 48).

We also examined the number of microvessels per cardiomyocyte. There was no difference in the number of microvessels between WT and *Epac1* KO at baseline (WT versus *Epac1* KO: 0.41 ± 0.02 versus 0.42 ± 0.04, n = 4, P = NS). However, the number was significantly decreased in WT compared with *Epac1* KO at 3 weeks after aortic banding (WT versus *Epac1* KO: 0.29 ± 0.01 versus 0.42 ± 0.04, n = 4, $P < 0.01$) (Figure 7, E and F).

Disruption of EPAC1 results in resistance to long-term ISO infusion. We also examined the effect of long-term ISO infusion on LV function (Supplemental Figure 16A). At 1 week after chronic ISO infusion, LVEF was significantly decreased in WT ($P < 0.01$), while it remained unchanged in *Epac1* KO (WT versus *Epac1* KO: from 70 ± 0.8 to 60 ± 1.1 versus from 62% ± 1.4% to 60% ± 0.9%, n = 14–31).

Cardiac fibrosis after long-term ISO infusion was also significantly decreased in *Epac1* KO (WT versus *Epac1* KO: 4.6% ± 1.6% versus 1.6% ± 0.2%, n = 5, $P < 0.01$) (Supplemental Figure 16, B and C). Similarly, cardiac apoptosis was also significantly attenuated in *Epac1* KO after long-term ISO infusion (WT versus *Epac1* KO: 0.49% ± 0.07% versus 0.24% ± 0.05%, n = 4–5, $P < 0.05$) (Supplemental Figure 16D).

The degree of cardiac hypertrophy was increased at 1 week, but remained similar in *Epac1* KO and WT (LV/tibial length ratio for WT versus *Epac1* KO: 5.7 ± 0.2 versus 5.9 ± 0.1, n = 14–15, P = NS; LV/BW ratio for WT versus *Epac1* KO: 3.5 ± 0.2 versus 3.7 ± 0.1, n = 14–15, P = NS) (Supplemental Figure 17, A and B).

Silencing of EPAC1 in cardiac fibroblasts did not alter cell proliferation. Since the mouse model is a global *Epac1* KO, the phenotype of less fibrosis after long-term ISO infusion or aortic banding may result from altered cell proliferation or signaling in cardiac fibroblasts. We thus examined the effect of silencing EPAC1 on neonatal rat cardiac fibroblast proliferation in response to ISO, using 3-(4,5-Dimethylthiazol-2-yl)-2,5-diphenyltetrazolium bromide (MTT) assay (Supplemental Figure 9B, Supplemental Figure 18, and ref. 49). Cardiac fibroblasts were cultured in medium with 10% fetal bovine serum for 24 hours and were starved for 48 hours without serum prior to stimulation. At 24 hours after ISO (1 μM or 10 μM) stimulation, MTT assay was performed. Cell proliferation was significantly increased ($P < 0.01$) by ISO (10 μM) from baseline (control siRNA versus EPAC1 siRNA: from 100% ± 5.7% to 137% ± 4.6% versus from 108% ± 1.7% to 140% ± 4.6%, n = 6–8), but the magnitudes of the increase were similar (P = NS) in cells transfected with control or EPAC1 siRNA (ref. 49 and Supplemental Figure 18A).

We also examined p44/42 MAPK (ERK1/2) phosphorylation on tyrosine- 202/threonine-204 and SRC phosphorylation on tyrosine-416 because phosphorylations of ERK1/2 and SRC are important for G protein–coupled receptor–mediated cardiac fibroblast proliferation (50). ERK1/2 phosphorylation and SRC phosphorylation were similar in both control and EPAC1 siRNA–treated cells (Supplemental Figure 18, B–D). However, both ERK1/2 and SRC phosphorylations were significantly ($P < 0.01$) increased in response to ISO (10 μM) in cells transfected with control or EPAC1

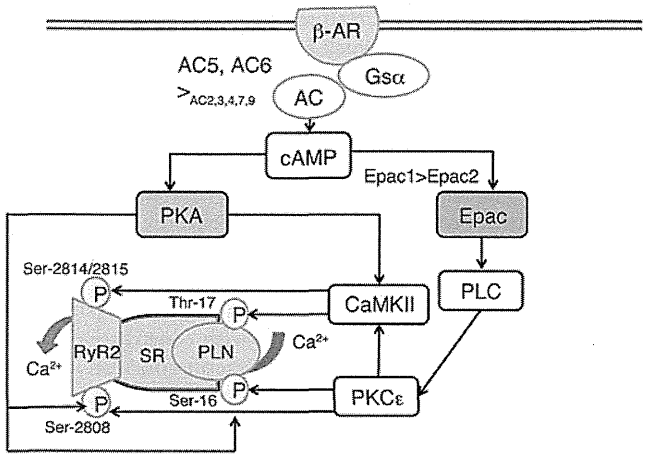

Figure 9

A schematic model of cAMP/EPAC signaling as opposed to cAMP/PKA signaling in the heart. Ca^{2+} stored in the SR is released into the cytosol to activate cardiac muscle contraction and subsequently reaccumulated to promote relaxation. PLN phosphorylation on serine-16 as well as threonine-17 occurs via the EPAC/PLC/PKCε/CaMKII pathway (27, 28). However, under physiological conditions, PLN phosphorylation on serine-16 by PKA rather than on threonine-17 by CaMKII is the major regulator of Ca^{2+} cycling in the heart (56, 57). Our current study indicates that PLN on serine-16 and RyR2 on serine-2808 and serine-2814 are phosphorylated by EPAC1 in addition to and independently of PKA or CaMKII. More importantly, hyperphosphorylation of PLN on serine-16 was recently reported to be associated not only with an increase in cardiac function in young animals (16, 17), but also with arrhythmia and cardiomyopathy after adrenergic stress, aortic banding, or ischemia (18, 20, 21). Our results suggest that *Epac1*-mediated hyperphosphorylation of PLN and RyR2 might be required for the development of heart failure as well as arrhythmia, in addition to PKA- or CaMKII mediated activation.

siRNA, and the magnitudes of their increase were similar in the 2 cases (ERK1/2: control siRNA versus EPAC1 siRNA: from 100 ± 2.5 to 151 ± 2.0 versus from 108% ± 3.7% to 154% ± 6.7%, $n = 4$; SRC: control siRNA versus EPAC1 siRNA: from 100% ± 2.5% to 233% ± 12% versus from 107% ± 9.7% to 235% ± 23%, $n = 7$-8). These data indicate that silencing EPAC1 in cardiac fibroblasts did not alter the cell-proliferative response to β-AR–signaling stimulation.

Disruption of EPAC1 results in resistance to aging-related cardiomyopathy. Key features of aging-related cardiomyopathy were examined, i.e., LV weight/tibial length ratio, LV function, apoptosis, and fibrosis. The LV weight/tibial length ratio was not different between old WT (5.6 ± 0.5) and old *Epac1* KO (5.6 ± 0.5) at baseline (24–32 months). However, aging-related changes of cardiac function (LVEF in WT versus *Epac1* KO: from 70% ± 0.8% [young] to 58% ± 1.3% [old] [$P < 0.01$] versus from 60% ± 1.1% to 58% ± 2.2%, P = NS) (Supplemental Figure 16E), fibrosis (old WT versus old *Epac1* KO: 3.2% ± 0.2% versus 1.2% ± 0.2%, $n = 5$–8, $P < 0.01$) (Supplemental Figure 16F) and apoptosis (old WT versus old *Epac1* KO: 0.38% ± 0.04% versus 0.22% ± 0.03%, $n = 5$, $P < 0.05$) (Supplemental Figure 16G) were all significantly decreased in *Epac1* KO.

Incidence of atrial fibrillation after rapid atrial pacing is attenuated in Epac1 KO. It has been reported that phosphorylations of RyR2 on serine-2814 and PLN on threonine-17 are increased after rapid atrial pacing in atrial myocytes and genetic inhibition of RyR2 phosphorylation on serine-2814 attenuates the incidence of atrial fibrillation (AF) induced by rapid atrial pacing (51). Accordingly, we examined the effects of *Epac1* deletion on the initiation and maintenance of AF in the mouse model (Figure 8 and ref. 52). Transesophageal rapid atrial pacing was performed at a cycle length of 30 ms for 1 minute, followed by measurement of the duration of pacing-induced AF (Figure 8A). In all WT control mice, AF was consistently induced for 50 to 60 seconds. In striking contrast, little (less than 4 seconds) or no AF was induced in *Epac1* KO. These data indicate that *Epac1* deletion may suppress the initiation and maintenance of AF after transesophageal rapid atrial pacing, probably through inhibition of hyperphosphorylation of RyR2 and/or PLN in atrial myocytes (AF duration for WT versus *Epac1* KO: 58 ± 3.8 versus 1.4 ± 1.4 seconds, $n = 4$–5, $P < 0.01$).

Catecholamine-mediated spontaneous activity in the pulmonary vein cardiomyocytes is attenuated in Epac1 KO. High-frequency focal activity in the pulmonary vein cardiomyocytes may contribute to arrhythmogenic activity, which is induced mostly via an increase of intracellular Ca^{2+} derived from SR (53, 54). The incidence of the spontaneous activity was not different in WT (4/17:24%) and *Epac1* KO (7/24:29%) at baseline (P = NS) (Supplemental Figure 19B). However, it was increased after noradrenaline (1 μM) treatment in both WT and *Epac1* KO, though its incidence was less in *Epac1* KO (12/17:71%) than in WT (15/15:100%) ($P < 0.05$ evaluated by Fisher's exact probability test). These finding indicated that catecholamine-mediated spontaneous activity in the pulmonary vein cardiomyocytes is attenuated in *Epac1* KO (Supplemental Figure 19, A and C).

Disruption of EPAC2 does not prevent the cardiac hypertrophy and the development of heart failure in response to pressure overload stress. In order to examine the effects of EPAC2, another cardiac isoform of EPAC, on the development of heart failure, we generated *Epac2* KO (Supplemental Figure 20). *Epac2* KO did not show any change in the size of the heart or in cardiac function, despite the smaller body weight, compared with that in WT (Supplemental Table 1). We examined PLN phosphorylation on serine-16 and on threonine-17 in *Epac2* KO, but the levels were similar in both WT and *Epac2* KO (Supplemental Figure 21).

In order to examine the role of EPAC2 in the development of heart failure, we performed aortic banding in *Epac2* KO and WT for 3 weeks. At baseline, there was no difference between WT and *Epac2* KO in the LV weight (mg)/tibial length (mm) (LV/tibial length ratio in WT versus *Epac2* KO: 5.7 ± 0.1 versus 5.2 ± 0.2 mg/mm, $n = 5$–7, P = NS). The degree of cardiac hypertrophy was significantly ($P < 0.01$) increased at 3 weeks, but the magnitudes of the increase were similar in both WT and *Epac2* KO (LV/tibial length ratio in WT versus *Epac2* KO: 7.1 ± 0.4 versus 6.8 ± 0.2, $n = 4$, P = NS) (Supplemental Figure 22A).

At 3 weeks after banding, cardiac function (LVEF) was significantly decreased in both WT and *Epac2* KO from baseline (WT versus *Epac2* KO: from 73% ± 1.1% to 55% ± 3.1% [$P < 0.01$, $n = 4$–5] versus from 72% ± 1.1% to 58% ± 5.2% [$P < 0.05$, $n = 5$–7]), but the magnitudes of the decrease were similar (P = NS) (Supplemental Figure 22B). LVESD was increased in both WT and *Epac2* KO at 3 weeks after banding (WT versus *Epac2* KO: from 2.7 ± 0.07 to 3.1 ± 0.2 [$P < 0.05$, $n = 4$–5] versus from 2.6 ± 0.05 to 3.1 ± 0.2 mm [$P < 0.05$, $n = 4$–13]), but the magnitudes of the increase were similar (P = NS) (Supplemental Figure 22C).

There was no difference in the degree of fibrosis between WT and *Epac2* KO at baseline (Supplemental Figure 22, D and E). Thus, the development of cardiac fibrosis was unaffected in *Epac2* KO (WT versus *Epac2* KO: 0.4% ± 0.08% versus 0.4% ± 0.09%, $n = 5$,

P = NS). Aortic banding increased the area of fibrosis in both WT and *Epac2* KO, but the magnitudes of the increase were similar (WT versus *Epac2* KO: 22% ± 3.6% versus 18% ± 5.3%, n = 4, P =NS) (Supplemental Figure 22, D and E).

Similarly, there was no difference in the number of TUNEL-positive cells between WT and *Epac2* KO at baseline (WT versus *Epac2* KO: 0.09% ± 0.02% versus 0.09% ± 0.01%, n = 5, P = NS) (Supplemental Figure 22F). Aortic banding significantly (P < 0.01) increased TUNEL-positive cells in both WT and *Epac2* KO, but the magnitudes of increase were similar (WT versus *Epac2* KO: 0.8% ± 0.04% versus 0.8% ± 0.05%, n = 4–5, P = NS) (Supplemental Figure 22F). These results indicate that *Epac2* KO did not show decreased cardiac contractility and PLN phosphorylation at baseline and did not show resistance after aortic banding, indicating that the cardioprotective effects of EPAC under stress such as pressure overload (Figures 5–7, Supplemental Figure 14, and Supplemental Figure 15), chronic catecholamine stress (Supplemental Figure 16, A–D), aging stress (Supplemental Figure 16, E–G), and AF susceptibility (Figure 8) are *Epac1* KO–specific phenotypes.

Discussion

RyR2 is a prominent regulator of systolic contraction and PLN is a prominent regulator of myocardial diastolic relaxation via modulation of the activity of the SERCA2a. Specifically, RyR2 in its phosphorylated state following the Ca^{2+} influx through the L-type Ca^{2+} channel is an accelerator of Ca^{2+} leakage from SR, and PLN in its dephosphorylated state is an inhibitor of Ca^{2+} transport to SR via SERCA2a, while phosphorylation of PLN removes this inhibition, indicating that both molecules have central roles in modulating Ca^{2+} homeostasis and, therefore, cardiac function (10, 11, 46).

Early studies of enhanced SR Ca^{2+} leakage in heart failure focused on PKA, a classic cAMP target. Recently, it has been shown that β-AR stimulation can also induce PKA-independent, i.e., CaMKII- or EPAC-mediated SR Ca^{2+} leakage in vitro by increasing RyR2 phosphorylation on serine-2814/2815 and PLN phosphorylation on threonine-17 via PLCε/PLCε/CaMKII signaling (27–30, 55). Nevertheless, key functional issues remain to be clarified because most previous studies relied on pharmacological stimulation with 8-CPT, an EPAC-selective but not isoform-selective cAMP analogue, which could have off-target effects (37). First, it is unknown whether these effects are mediated by EPAC1 or EPAC2. Second, it is unknown whether EPAC-regulated Ca^{2+} homeostasis is important for cardiac function and arrhythmogenesis under physiological conditions. Third, it remains unknown whether EPAC regulates PLN phosphorylation on serine-16 in addition to threonine-17, which is known to be a major regulator of Ca^{2+} cycling in the heart and closely associated not only with an increase in cardiac function (16, 17, 56, 57), but also with arrhythmia and cardiomyopathy after chronic catecholamine infusion, aortic banding, or ischemia (18, 20, 21). We thus generated *Epac1* KO and *Epac2* KO in addition to silencing EPAC1 with siRNA and selectively inhibiting PKA with Ad-PKI-GFP in cardiac myocytes. The results clearly demonstrated that EPAC1-regulated Ca^{2+} homeostasis via PLN phosphorylation on serine-16, together with RyR2 phosphorylation on serine-2808 and serine-2814, may cause transition from hypertrophy to heart failure and evoke susceptibility to arrhythmia (Figure 9 and refs. 21, 58).

Pln-null mice show no gross developmental abnormalities, but exhibit enhanced myocardial contractility owing to increased SERCA2a pump activity and higher SR Ca^{2+} load in cardiomyocytes (12). Ablation of PLN restored contractility in some cardiomyopathic mouse models, such as cardiac-specific calsequestrin overexpression, targeted disruption of muscle-specific LIM protein, or cardiac-specific β_1-AR overexpression (16, 17, 59). Thus, various therapeutic approaches targeting or inhibiting PLN have been examined to rescue the failing heart (60, 61).

However, it was subsequently reported that ablation of PLN shows no cardioprotective effect against chronic pressure overload or ischemic injury and, indeed, exacerbates cardiac dysfunction in mice with cardiac CaMKIIδc overexpression, even if the Ca^{2+} transient is improved (19). More recently, it was reported that hyperphosphorylation of PLN in mice with constitutively active phosphatase inhibitor-1 increased contractile function in young animals, but also resulted in increased susceptibility to arrhythmias and cardiomyopathy in response to chronic catecholamine stress and aging, probably through increased Ca^{2+} leakage, leading to arrhythmogenicity and cardiomyocyte apoptosis (21). Our current data obtained in *Epac1* KO and *Epac2* KO demonstrated that EPAC1 plays an important role in PLN phosphorylation on serine-16 and EPAC1-mediated PLN phosphorylation rather than PKA-mediated PLN phosphorylation might have a pivotal role in the development of heart failure in response to chronic pressure overload, catecholamine stress, and aging, because the PKA pathway remains intact in *Epac1* KO.

For many decades, it has been believed that the major target of catecholamine/cAMP signaling is PKA. Although acute sympathetic stimulation and activation of the cAMP/PKA pathway represent a major mechanism of improvement of cardiac function, previous studies by us and other groups using transgenic models have demonstrated that chronic activation of these pathways arising from specific cardiac overexpression of β-AR, Gsα, and PKA results in cardiomyopathy (3–5). On the other hand, disruption of type 5 AC, a major cardiac AC isoform, protects the heart from chronic pressure overload and catecholamine stress without affecting baseline cardiac function in mice (6–8). Interestingly, our results indicate that cardiac function is preserved in response to chronic pressure overload, chronic catecholamine, and aging stress in *Epac1* KO, indicating that both phosphorylation of PLN on serine-16 and phosphorylation of RyR2 on serine-2808 and serine-2814 by EPAC1, rather than PKA, might be essential for the transition of hypertrophy to heart failure in response to chronic activation of β-AR signaling (11, 46, 58, 62).

Increased Ca^{2+} leakage in atrial myocytes has been demonstrated to be a cause and consequence of AF, but the mechanism remains poorly understood (63). Recently, it was demonstrated that PLN phosphorylation on serine-16, rather than threonine-17, was significantly increased in the atrium of chronic AF patients while PKA phosphorylation of inhibitory troponin subunit was unaltered (22). Similarly, it was demonstrated that rapid atrial pacing induces phosphorylation of RyR2 on serine-2814 and PLN on threonine-17 and genetic inhibition of RyR2 phosphorylation on serine-2814 prevents AF after rapid atrial pacing (64). These results indicate that altered Ca^{2+} homeostasis in atrial myocytes through EPAC-mediated hyperphosphorylation of PLN and RyR2 may cause susceptibility to AF. We thus hypothesized that EPAC1 plays an important role in the occurrence of AF, and we confirmed this idea using a transesophageal pacing-induced AF mouse model. American College of Cardiology, American Heart Association, and European Society of Cardiology guidelines strongly recommend β-blockers for the management of adrenergically induced AF, but it is difficult

to use β-blockers in patients with chronic obstructive pulmonary disease or severe heart failure. Therefore, EPAC may be available as a new target of pharmacotherapy for adrenergically induced AF (65).

PLN was demonstrated to be phosphorylated by PKC in vitro in addition to PKA and CaMKII (39, 41), but the mechanism of PKC-dependent PLN phosphorylation remains unclear and its importance for cardiac function is controversial (66, 67). Our current in vitro studies, in agreement with earlier studies (27–29), indicate that EPAC regulates PLN phosphorylation on both serine-16 and threonine-17 through PLC/PKCε signaling. However, our in vivo studies using *Epac1* KO show that EPAC1 regulates PLN phosphorylation on serine-16 at baseline and under stress, but it does not affect the phosphorylation on threonine-17. Previous in vitro studies have shown that serine-16 of PLN and threonine-17 of PLN can be readily and independently phosphorylated by PKA and CaMKII, respectively. However, previous in vivo studies indicated that PLN phosphorylation on threonine-17 can be induced by β-AR stimulation that is sufficient to increase cytosolic Ca^{2+} concentration, which in turn would activate CaMKII and/or inhibit the phosphatase that dephosphorylates PLN. The apparent difference between in vitro and in vivo PLN phosphorylation is yet to be reconciled (68), but a possible explanation of the difference between our in vitro and in vivo data on PLN phosphorylation at threonine-17 is that the extent of CaMKII activation was not enough to produce a significant difference between WT and *Epac1* KO under β-AR stimulation in response to ISO in the Langendorf-perfused heart system used in this study. We also cannot exclude the possibility that this might be due to a difference in the specificity of the gene-silencing technique in vitro with siRNA and in vivo with genetic KO because complete gene silencing can be achieved by genetic KO (31), but not by using siRNA (Supplemental Figure 9 and ref. 69).

In contrast with *Epac1* KO, disruption of EPAC2 does not alter the cardiac function or PLN phosphorylation at baseline and has no protective effects after aortic banding. These data indicate that EPAC1, but not EPAC2, is a major regulator of cardiac function at baseline and under stress.

More importantly, cardiac function and the Ca^{2+} transient are similar in global *Plce* KO and WT at baseline even if the ISO-stimulated Ca^{2+} transient is smaller in *Plce* KO (70). Global *Plce* KO does not show a protective phenotype against chronic catecholamine stress (70) in contrast with *Epac1* KO. Otherwise, global *Plce* KO is more susceptible than WT to the development of cardiac hypertrophy and fibrosis after chronic ISO infusion (70). In contrast with global *Plce* KO, myocyte-specific *Plce* KO is not susceptible, but is rescued from cardiac hypertrophy as well as cardiac dysfunction after TAC (71). Also, PLCε was demonstrated to generate a multifunctional complex with muscle-specific A-kinase–anchoring protein at or near the nuclear envelope along with *Epac1*, PKCε, PKD, and RyR2 in cardiac myocytes (71). Pkce KO does not show a protective phenotype and is not susceptible to development of cardiac hypertrophy after TAC, in contrast with global *Plce* KO and myocyte-specific *Plce* KO (72). These data indicate that disruption of EPAC1 modulates or antagonizes the downstream PLCε/PKCε pathway, which in turn is associated with the cardioprotective phenotype of *Epac1* KO under stress.

During the revision of this manuscript, another group reported that cardiac function was not different between WT and *Epac1* KO at baseline in contrast with our findings. The reason for the difference of the cardiac phenotype between our *Epac1* KO and that generated by the other group is not clear (30). However, the genetic backgrounds of *Epac1* KO generated by us (CBA-C57BL/6) and by the other group (R1-C57BL/6) were different, and this might cause the difference in the mouse phenotype (73, 74), as in the case of type 5 AC KO (129/SvJ-C57BL/6) generated by us (6, 7) and another group (C57BL/6) (75) and *Plce* KO generated by 2 different groups: 129/Sv-C57BL/6 (76) versus 129/S6-C57B/6 (70). Also, environmental influences have been reported to alter phenotype, as in the case of *Tgfb* KO (77, 78), and we cannot exclude this as another possibility.

In summary, we have demonstrated that disruption of EPAC1 protects the heart from chronic pressure overload, chronic catecholamine stress, aging-related cardiomyopathy, and AF susceptibility through the inhibition of PLN phosphorylation on serine-16 in addition to the inhibition of RyR2 phosphorylation on serine-2808 and serine-2814. The cAMP/PKA pathway is believed to be a major pathway for the development of heart failure as well as arrhythmia (5, 21). Our present data show that the cAMP/EPAC1 pathway plays an important role independently of the cAMP/PKA pathway in the development of heart failure and arrhythmia.

Methods

Reagents. All chemicals were obtained from Sigma-Aldrich, except 8-CPT-AM (Biolog Life Science Institute) and Indo-1/AM (Dojindo Laboratories).

Mice. Generation of *Epac1* KO has been previously reported (31). *Epac2* KO were similarly generated by means of homologous recombination. Briefly, the targeting vector was constructed by inserting pENTR loxP/PGK-Neo-pA/loxP (Laboratory for Animal Resources and Genetic Engineering [LARGE]; http://www.cdb.riken.jp/arg/cassette.html) into exon 1 and intron 1 of the genomic *Epac2* locus (Supplemental Figure 20A). The targeting vector was introduced into TT2 embryonic stem cells (79), and homologous recombinant clones were first identified by PCR, then confirmed by Southern blot analysis (Supplemental Figure 20B and refs. 6, 31). The targeted embryonic stem cell clones were injected into CD 18-cell–stage embryos, and the resultant male chimeras were mated with C57BL/6 females to establish germ line transmission. All experiments were performed on C57BL/6 and CBA mixed background 3- to 5-month-old male homozygous *Epac2* KO and WT littermates from F1 heterozygote crosses. Mice were genotyped by PCR using a mixture of 2 primer sets (F1, TGGGTGGGTGGTTTCCAATG; B1, CCTAACACAGACCTTGAGAGAGCG; F2, TCGTGCTTTACGGTATCGCCGCTCCCGATT; B2, CGTAGCTCCAATCCTTCCATTCA). The PCR conditions consisted of 95°C for 5 minutes, 35 cycles of 95°C for 30 seconds each, 60°C for 30 seconds, and 72°C for 30 seconds, followed by 72°C for 7 minutes (Supplemental Figure 20C). mRNA expression of the *Epac* isoforms (*Epac1* and *Epac2*) in the heart of *Epac2* KO was examined by Northern blot analysis (Supplemental Figure 20D and ref. 80).

All experiments were performed on 3- to 6-month-old homozygous KO (*Epac1*, *Epac2*) mice and WT littermates.

Western blotting. Hearts were removed from each animal or Langendorf apparatus, snap-frozen in liquid nitrogen, and stored at –80°C after physiological studies. Crude cardiac membrane fraction or whole -issue homogenate was prepared, separated on 6% to 15% SDS-polyacrylamide gel and blotted onto nitrocellulose membrane. Western blotting was conducted using commercially available antibodies. β_1-AR, β_2-AR, βARK, Gβ, Gq, type 5/6 AC (AC5/6), and PKA-catalytic subunit antibodies were purchased from Santa Cruz Biotechnology Inc. Gsα and Giα antibodies were purchased from PerkinElmer. PLN, PLN phosphorylated on serine-16 and threonine-17, RYR2, and RYR2 on serine-2808 and serine-2814 were purchased from Badrilla. Antibodies to PKA regulatory subunits (RIIα and R1α) were purchased from BD Transduction Laboratories. EPAC1, EPAC2, CaMKII, phospho-CaMKII (threonine-286), ERK1/2, phospho-ERK1/2

(tyrosine-202/threonine-204), SRCc, and phospho-SRC (tyrosine-416) antibodies were purchased from Cell Signaling Technology. SERCA2a antibody was purchased from Thermo Scientific. Expression of proteins was quantified by densitometry.

Real-time quantitative PCR. Total RNA was extracted using TRIzol Reagent (Life Technologies) according to the manufacturer's protocol. RNA concentration and quality were determined by spectrophotometry. To remove contaminating genomic DNA, samples were treated with DNase I (Life Technologies). Total RNA was reverse-transcribed with SuperScript First-Strand Synthesis System for RT-PCR kit (Life Technologies) according to the manufacturer's instructions.

mRNA expression of *Pkca*, *Pkcb*, *Pkcd*, *Pkcg*, and *Pkce* was quantified by quantitative real-time PCR using the ABI-PRISM 7700 Sequence Detection System with SYBR Green. The primer pairs for each subtype of PKC were as follows:

Pkca, forward, 5′-GCCGCAGTGTCGTTATGAAAGTA-3′, reverse, 5′-GCTCCATGTGTGCCATTCAATTAG-3′; *Pkcb*, forward, 5′-AAGACATTCTGTGGCACTCCAGAC-3′, reverse, 5′-AGCCAACATTTCATACAGCAGGAC-3′; *Pkcd*, forward, 5′-CAAAGGCCGCTTCGAACTCTAC-3′, reverse, 5′-GGCCATCCTTGTCCAGCATTAC-3′; *Pkcg*, forward, 5′-CACAGACTTCGGCATGTGTAAAGA-3′, reverse, 5′-CCATAGGGCTGATAGGCAAATGA-3′; and *Pkce*, forward, 5′-ATGGCGTGACAACTACCACCTTC-3′, reverse, 5′-CCGGCCATCATCTCGTACATC-3′. The amount of each subtype mRNA was normalized to that of 18S rRNA to obtain the relative amount.

Neonatal cardiac myocyte/fibroblast preparation and transfection of siRNA. Primary cultures of neonatal rat or mouse cardiomyocytes or fibroblast were prepared (81–83). Double-stranded siRNA to the selected region of each subtype of PKC (α, β, ε, δ, γ), EPAC1, and negative siRNA (control) were purchased from QIAGEN. At 48 hours after plating, cultured neonatal rat cardiac myocytes/fibroblasts (1.2×10^5 cells per 24-mm plate) were transfected with siRNA using Lipofectamine RNAiMAX (Life Technologies), according to the manufacturer's instructions.

Briefly, siRNA (20 nM) in 50 μl of OptiMEM I medium (Life Technologies) and 0.5 μl of Lipofectamine RNAiMAX (Life Technologies) in 50 μl OptiMEM I medium were mixed and then added to the dishes. At 24 hours after transfection, the culture medium (minimum essential medium) was replaced with fresh medium and incubation was continued for 24 hours in a humidified atmosphere of 5% CO_2 in air at 37°C. ISO treatment was performed at 1 μM (mouse) or 10 μM (rat), which was chosen based on preliminary experiments performed with reference to previous studies on PLN phosphorylation (70, 84). The efficiency of knockdown of each subtype of PKC was evaluated at 24 to 48 hours after transfection by means of real-time quantitative PCR. Negative siRNA used as a control was purchased from QIAGEN (Cat no. 1027281). The siRNA sequences of PKC subtype were as follows: PKCα, forward, 5′-GAAGGGUUCUCGUAUGUCATT-3′, reverse, 5-UGACAUACGAGAACCCUUCAA-3′; PKCβ, forward, 5′-GAAGAAGGCGAGUACUUUATT-3′, reverse, 5′-UAAAGUACUCGCCUUCUUCCT-3′; PKCδ, forward, 5′-CCUUUAAGCCCAAAGUGAATT-3′, reverse, 5′-UUCACUUUGGGCUUAAAGGGC-3′; PKCγ, forward, 5′-GGGCGAGUAUUACAAUGUATT-3′, reverse, 5′-UACAUUGUAAUACUCGCCCTC-3′; and PKCε, forward, 5′-CGAUGAGUUCGUCACUGAUTT-3′, reverse, 5′-AUCAGUGACGAACUCAUCGTG-3′.

Generation of adenovirus. A DNA oligo corresponding to the coding sequence for amino acids 1–25 (MTDVETTYADFIASGRTGRRNAIHD) of mouse protein kinase (cAMP-dependent, catalytic) inhibitor α (*Pkia*) (mouse Entrez Gene ID 18767) was synthesized. Recombinant adenovirus encoding PKIα-GFP infusion gene was generated using the AdEasy system (44).

Adult mouse ventricular myocytes preparation. Adult mouse ventricular myocytes were prepared from mice by Langendorf perfusion and collagenase digestion, as described (45, 85, 86).

Measurement of intracellular Ca^{2+}. Intracellular Ca^{2+} was measured with Indo-1, as in our previous study (87). The cells were preincubated at 37°C with the acetoxymethyl derivative of Indo-1 (Indo-1/AM 10 μM, 45 minutes) in the experimental chamber. After preincubation, the chamber was placed on a fluorescence microscope (Olympus IX70; Olympus Corp.) and perfused with HEPES-Tyrode solution as described above. Ca^{2+} transients were evoked at 1 Hz through platinum wire pairs with rectangular current pulses of 3 ms duration generated by an electrical stimulator (SEN-3303; Nihon Kohden). The cells were excited at 360 nm with an Axenon lamp, and the emission bands at 395 to 415 nm and 470 to 490 nm (Indo-1) were separated by means of dichroic mirrors (W-VIEW system; Hamamatsu Photonics) and detected with a high-speed cooled CCD camera (C6790; Hamamatsu Photonics) at a time resolution of 1.95 ms.

The ratio of emission between short-wavelength fluorescence and long-wavelength fluorescence was calculated (Aquacosmos software; Hamamatsu Photonics). In situ calibration of Indo-1 fluorescence ratio values to intracellular Ca^{2+} concentration was performed as described previously (87). The time constant (τ) for the Ca^{2+} transient decay was obtained by fitting the decay of the transients to a single exponential equation: $Y(t) = a \times \exp -k \times t + b$, where a = Ca^{2+} transient amplitude; b = baseline value; k is the rate coefficient. k was obtained from the fitting, and τ was calculated as $\tau = 1/k$.

Measurement of contractile force. Myocardial contractile force was measured as previously described (88). RV free wall strips (approximate length and width: 4 and 2 mm, respectively) were rapidly isolated from mice anesthetized with ether. Preparations were placed horizontally in a 20 ml organ bath containing modified Ringer solution of the following composition: 135 mM NaCl, 5 mM KCl, 2 mM $CaCl_2$, 1 mM $MgCl_2$, 15 mM $NaHCO_3$, and 5.5 mM glucose (pH 7.4 at 36°C). The solution was gassed with 95% O_2–5% CO_2 and maintained at 35–36°C. The preparations were driven by a pair of platinum plate electrodes (field stimulation) with rectangular current pulses (1 Hz, 3 ms, 1.5× threshold voltage) generated by an electronic stimulator. Developed tension was recorded isometrically with a force-displacement transducer connected to a minipolygraph.

Patch-clamp recording. The L-type Ca^{2+} channel current (I_{CaL}) was measured as described, with minor modifications (89, 90). Briefly, I_{CaL} was measured in the whole-cell patch-clamp configuration with EPC8 (HEKA) via an A/D converter, Digidata1440A, and Clampex 10.0 (Axon Instrument) at room temperature. Data were analyzed by Clampfit 10.0 (Axon Instrument) and GraphPad Prism 4 (GraphPad Software). Patch -pipettes were fabricated from borosilicate glass and had tip resistance of 1.2–2.2 MΩ when filled with pipette solution containing the following: 120 mM CsCl; 20 mM tetraethylammonium chloride; 5 mM adenosine 5′-triphosphate magnesium salt; 5 mM creatine phosphate disodium salt; 0.2 mM guanosine 5′-triphosphate; 14 mM EGTA; 10 mM Hepes; titrated to pH 7.3 with CsOH. The extracellular solution contained the following: 137 mM NaCl; 5.4 mM KCl, 10 mM HEPES, 1 mM $MgCl_2$, 10 mM glucose, 2 mM $CaCl_2$, 0.01 mM tetrodotoxin; titrated to pH 7.4 with NaOH. I_{K1}, the inward rectifier K^+ current, was suppressed by the addition of $BaCl_2$ at 0.2 mM to the extracellular solution. The extracellular solution surrounding the patch-clamped cell was rapidly changed by a custom-made concentration clamp system (91). I_{CaL} was isolated as the current component blocked by $CdCl_2$ at 0.2 mM.

The Na^+-Ca^{2+} exchange current (I_{NCX}) was measured with pipette solution containing the following: 50 mM CsOH; 10 mM Cs-methanesulfonate; 10 mM TEA-Cl; 20 mM NaCl; 5 mM Mg^{2+}-ATP; 10 mM HEPES; 20 mM BAPTA; 10 mM $CaCl_2$ (226 nM free Ca^{2+}); titrated to pH 7.3 with CsOH. Extracellular solution contained the following: 137 mM NaCl, 5.4 mM CsCl, 10 mM HEPES, 1 mM $MgCl_2$, 10 mM glucose, 2 mM $CaCl_2$, 0.01 mM tetrodotoxin, 0.2 mM $BaCl_2$, 10 mM 4-AP, 0.01 mM nitrendipine, 0.1 mM niflumic acid, 0.005 mM ryanodine; titrated to pH 7.4 with NaOH. In order to exclude the secondary effect of intracellular Ca^{2+} handling on I_{NCX}, the concentration of free

Ca^{2+} was buffered with a high concentration of BAPTA. I_{NCX} was recorded by applying ramp pulse ranging from 80 mV to -150 mV for 100 ms following step pulses to -40 mV for 40 ms and to 0 mV for 10 ms to inactivate I_{Na} and I_{CaL}, respectively, from the holding potential of -70 mV. I_{NCX} was isolated as the current component blocked by $NiCl_2$ at 5 mM.

Physiological studies. Mice were anesthetized with isoflurane vapor titrated to maintain the lightest anesthesia possible. On average, 1.5% vol/vol isoflurane vapor was required to maintain adequate anesthesia. Echocardiographic measurements and invasive hemodynamic measurements were performed (6–8, 92). Intravenous infusion of ISO (0 to 0.40 μg/kg/min for 5 minutes) was performed using an infusion pump (6, 8). Transverse aortic banding and long-term infusion of ISO were performed for 7 days at 60 mg/kg/d as described previously by us (7, 8). ECG recordings of awake, free-moving mice were obtained using a telemetric method (PhysioTel; Data Science International). AF was induced by transesophageal rapid atrial pacing in mice as described previously (52).

Histological analysis. Heart specimens were fixed with formalin, embedded in paraffin, and sectioned at 6-μm thickness. Interstitial fibrosis was evaluated by Masson trichrome staining using the Accustatin Trichrome Stain Kit (Sigma-Aldrich). DNA fragmentation was detected in situ by TUNEL staining as described previously (7, 8). Frozen cross sections of the heart samples were immunohistochemically double-stained by the use of antibodies against PECAM (BD Biosciences — Pharmingen) and dystrophin (Novocastra Laboratories). The number of microvessels per cardiomyocyte was calculated as described previously (48).

Proliferation assay. MTT cell viability assay was used to measure neonatal rat cardiac fibroblast proliferation using Cell Proliferation Kit I according to the manufacturer's instructions (Roche) (49). Briefly, cardiac fibroblast were seeded onto 96-well tissue culture plates (1×10^3 cells per well) in DMEM with 10% fetal bovine serum for 24 hours and starved for 48 hours with 1% bovine serum albumin prior to stimulation. ISO (1 μM or 10 μM) was added to the medium. At 24 hours after incubation, the supernatants were aspirated, 10 μl of MTT solution (5 mg/ml) was added to each well, and incubation was continued for 4 hours. After incubation, the supernatants were aspirated and 100 μl of 10% SDS in 10 mM HCl was added. The amount of metabolized MTT was determined with a microplate reader.

Recording of spontaneous activity in myocardial sleeves of pulmonary veins. Pulmonary veins were separated from the atrium at the left atrium–pulmonary vein junction and separated from the lungs at the end of the pulmonary vein myocardial sleeves. Tubular pulmonary veins were cut open and pinned down, endocardial side up, on the bottom of the 20-ml recording chamber. The extracellular solution contained the following: 118.4 mM NaCl, 4.7 mM KCl, 2.5 mM $CaCl_2$, 1.2 mM $MgSO_4$, 1.2 mM KH_2PO_4, 24.9 mM $NaHCO_3$, and 11.1 mM glucose, pH 7.4); it was gassed with 95% O_2–5% CO_2 and maintained at 36 ± 0.5°C. Action potentials were recorded in pulmonary vein tissue preparations by using standard microelectrodes inserted from the luminal side. The glass microelectrodes filled with 3M KCl had resistances of 20 to 30 MΩ. The output of a microelectrode amplifier with high input impedance and capacity neutralization (MEZ8201; Nihon Kohden) was digitized by an A/D-converting interface (Power Lab/4SP, AD Instruments) and analyzed using Chart 7 soft ware (AD Instruments) (93, 94).

Statistics. All data are reported as mean ± SEM. Comparison of data was performed using a 2-tailed Student's *t* test when 2 samples were considered or 1-way ANOVA for 3 or more samples. Fisher's exact probability test was used to examine the incidence of spontaneous activity in pulmonary vein myocytes. Differences were considered significant at $P < 0.05$.

Study approval. This study was approved by the Animal Care and Use Committee at Yokohama City University School of Medicine.

Acknowledgments

This study was supported in part by grants from the Ministry of Health, Labor and Welfare (to Y. Ishikawa), and a Grant-in-Aid for Scientific Research on Innovative Areas (22136009) as well as grants from the Kitsuen Kagaku Research Foundation (to Y. Ishikawa), the Japanese Ministry of Education, Culture, Sports, Science, and Technology (to Y. Ishikawa [24390200, 259670131], S. Okumura [60233475], T. Fujita [40468202], M. Jin [postdoctoral fellowship for foreign researchers 2011.9-2013.8], I. Namekata [25860194], Y. Mototani [22791147], M. Sato [24590280, 25136721], U. Yokoyama [25293236], S. Suzuki [21790208], R. Kurotani [24591151], Y. Bai [22790719], T. Tsunematsu [22590811], Y. Ichikawa [25860614], S. Adachi-Akahane [23659142], H. Tanaka [24590334]), the Japan Space Forum (to Y. Ishikawa), the Takeda Science Foundation (to Y. Ishikawa and S. Okumura), the Yokohama Foundation for Advancement of Medical Science (to S. Okumura and Y. Ohnuki), a grant for a 2006–2007 Strategic Research Project (no. K19027) from Yokohama City University, Japan (to S. Okumura), the Mitsubishi Pharma Research Foundation (to S. Okumura), Research for Promoting Technological Seeds A (discovery type) (to S. Okumura), the Yokohama Academic Foundation (to S. Okumura and Y. Ohnuki), the 2010 Commercialization Promotion Program for Biotechnology-Related Studies (to S. Okumura), and Grants for Research and Development Project II (nos. 8 and 14) from Yokohama City University (to Y. Ishikawa and S. Okumura), and the Research Foundation for Community Medicine (to S. Okumura).

Received for publication May 23, 2012, and accepted in revised form February 27, 2014.

Address correspondence to: Satoshi Okumura, Department of Physiology, Tsurumi University School of Dental Medicine, 2-1-2 Tsurumi, Tsurumi-ku, Yokohama 230-8501, Japan. Phone: 81.45.580.8476; Fax: 81.45.585.2889; E-mail: okumura-s@tsurumi-u.ac.jp. Or to: Yoshihiro Ishikawa, Cardiovascular Research Institute, Yokohama City University Graduate School of Medicine, 3-9 Fukuura, Kanazawa-ku, Yokohama 236-0004, Japan. Phone: 81.45.787.2575; Fax: 81.45.788.1470; E-mail: yishikaw@yokohama-cu.ac.jp.

1. Ishikawa Y, Homcy CJ. The adenylyl cyclases as integrators of transmembrane signal transduction. *Circ Res.* 1997;80(3):297–304.
2. Vatner DE, et al. β-adrenergic receptor-G protein-adenylyl cyclase signal transduction in the failing heart. *Am J Cardiol.* 1999;83(12A):80H–85H.
3. Engelhardt S, Hein L, Wiesmann F, Lohse MJ. Progressive hypertrophy and heart failure in β_1-adrenergic receptor transgenic mice. *Proc Natl Acad Sci U S A.* 1999;96(12):7059–7064.
4. Asai K, et al. β-adrenergic receptor blockade arrests myocyte damage and preserves cardiac function in the transgenic Gsα mouse. *J Clin Invest.* 1999; 104(5):551–558.
5. Antos CL, et al. Dilated cardiomyopathy and sudden death resulting from constitutive activation of protein kinase a. *Circ Res.* 2001;89(11):997–1004.
6. Okumura S, et al. Type 5 adenylyl cyclase disruption alters not only sympathetic but also parasympathetic and calcium-mediated cardiac regulation. *Circ Res.* 2003;93(4):364–371.
7. Okumura S, et al. Disruption of type 5 adenylyl cyclase gene preserves cardiac function against pressure overload. *Proc Natl Acad Sci U S A.* 2003; 100(17):9986–9990.
8. Okumura S, et al. Disruption of type 5 adenylyl cyclase enhances desensitization of cyclic adenosine monophosphate signal and increases Akt signal with chronic catecholamine stress. *Circulation.* 2007; 116(16):1776–1783.
9. Yan L, et al. Type 5 adenylyl cyclase disruption increases longevity and protects against stress. *Cell.* 2007;130(2):247–258.
10. Koss KL, Kranias EG. Phospholamban: a prominent regulator of myocardial contractility. *Circ Res.* 1996; 79(6):1059–1063.
11. Li J, et al. β-adrenergic stimulation increases RyR2 activity via intracellular Ca^{2+} and Mg^{2+} regulation. *PLoS One.* 2013;8(3):e58334.

12. Luo W, et al. Targeted ablation of the phospholamban gene is associated with markedly enhanced myocardial contractility and loss of β-agonist stimulation. *Circ Res.* 1994;75(3):401–409.
13. Kuschel M, Karczewski P, Hempel P, Schlegel WP, Krause EG, Bartel S. Ser^{16} prevails over Thr^{17} phospholamban phosphorylation in the β-adrenergic regulation of cardiac relaxation. *Am J Physiol.* 1999; 276(5 pt 2):H1625–H1633.
14. Sordahl LA, McCollum WB, Wood WG, Schwartz A. Mitochondria and sarcoplasmic reticulum function in cardiac hypertrophy and failure. *Am J Physiol.* 1973;224(3):497–502.
15. Whitmer JT, Kumar P, Solaro RJ. Calcium transport properties of cardiac sarcoplasmic reticulum from cardiomyopathic Syrian hamsters (BIO 53.58 and 14.6): evidence for a quantitative defect in dilated myopathic hearts not evident in hypertrophic hearts. *Circ Res.* 1988;62(1):81–85.
16. Minamisawa S, et al. Chronic phospholamban-sarcoplasmic reticulum calcium ATPase interaction is the critical calcium cycling defect in dilated cardiomyopathy. *Cell.* 1999;99(3):313–322.
17. Sato Y, et al. Rescue of contractile parameters and myocyte hypertrophy in calsequestrin overexpressing myocardium by phospholamban ablation. *J Biol Chem.* 2001;276(12):9392–9399.
18. Cross HR, Kranias EG, Murphy E, Steenbergen C. Ablation of PLB exacerbates ischemic injury to a lesser extent in female than male mice: protective role of NO. *Am J Physiol Heart Circ Physiol.* 2003; 284(2):H683–H690.
19. Zhang T, et al. Phospholamban ablation rescues sarcoplasmic reticulum Ca^{2+} handling but exacerbates cardiac dysfunction in CaMKIIδc transgenic mice. *Circ Res.* 2010;106(2):354–362.
20. Kiriazis H, et al. Hypertrophy and functional alterations in hyperdynamic phospholamban-knockout mouse hearts under chronic aortic stenosis. *Cardiovasc Res.* 2002;53(2):372–381.
21. Wittkopper K, et al. Constitutively active phosphatase inhibitor-1 improves cardiac contractility in young mice but is deleterious after catecholaminergic stress and with aging. *J Clin Invest.* 2010; 120(2):617–626.
22. El-Armouche A, et al. Molecular determinants of altered Ca^{2+} handling in human chronic atrial fibrillation. *Circulation.* 2006;114(7):670–680.
23. Kawasaki H, et al. A family of cAMP-binding proteins that directly activate Rap1. *Science.* 1998; 282(5397):2275–2279.
24. de Rooij J, et al. Epac is a Rap1 guanine-nucleotide-exchange factor directly activated by cyclic AMP. *Nature.* 1998;396(6710):474–477.
25. Gloerich M, Bos JL. Epac: defining a new mechanism for cAMP action. *Annu Rev Pharmacol Toxicol.* 2010; 50:355–375.
26. Morel E, et al. cAMP-binding protein Epac induces cardiomyocyte hypertrophy. *Circ Res.* 2005; 97(12):1296–1304.
27. Oestreich EA, et al. Epac-mediated activation of phospholipase Cε plays a critical role in β-adrenergic receptor-dependent enhancement of Ca^{2+} mobilization in cardiac myocytes. *J Biol Chem.* 2007;282(8):5488–5495.
28. Oestreich EA, et al. Epac and phospholipase Cε regulate Ca^{2+} release in the heart by activation of protein kinase Cε and calcium-calmodulin kinase II. *J Biol Chem.* 2009;284(3):1514–1522.
29. Smrcka AV, Oestreich EA, Blaxall BC, Dirksen RT. EPAC regulation of cardiac EC coupling. *J Physiol.* 2007;584(pt 3):1029–1031.
30. Pereira L, et al. *Epac2* mediates cardiac β1-adrenergic-dependent sarcoplasmic reticulum Ca^{2+} leak and arrhythmia. *Circulation.* 2013; 127(8):913–922.
31. Suzuki S, et al. Differential roles of Epac in regulating cell death in neuronal and myocardial cells. *J Biol Chem.* 2010;285(31):24248–24259.
32. Lindemann JL, Jones LR, Hathaway DR, Henry BG, Watanabe AM. β-adrenergic stimulation of phospholamban phosphoralation and Ca^{2+}-ATPase activity in guinea pig ventricle. *J Biol Chem.* 1983; 258(1):464–471.
33. Vliem MJ, et al. 8-pCPT-2′-O-Me-cAMP-AM: an improved Epac-selective cAMP analogue. *Chembiochem.* 2008;9(13):2052–2054.
34. Brette F, Blandin E, Simard C, Guinamard R, Salle L. Epac activator critically regulates action potential duration by decreasing potassium current in rat adult ventricle. *J Mol Cell Cardiol.* 2013;57:96–105.
35. Chang CW, Chang GD, Chen H. A novel cyclic AMP/Epac1/CaMKI signaling cascade promotes GCM1 desumoylation and placental cell fusion. *Mol Cell Biol.* 2011;31(18):3820–3831.
36. Laxman S, Riechers A, Sadilek M, Schwede F, Beavo JA. Hydrolysis products of cAMP analogs cause transformation of Trypanosoma brucei from slender to stumpy-like forms. *Proc Natl Acad Sci U S A.* 2006;103(50):19194–19199.
37. Poppe H, et al. Cyclic nucleotide analogs as probes of signaling pathways. *Nat Methods.* 2008;5(4):277–278.
38. Hammond J, Balligand JL. Nitric oxide synthase and cyclic GMP signaling in cardiac myocytes: from contractility to remodeling. *J Mol Cell Cardiol.* 2012; 52(2):330–340.
39. Movsesian MA, Nishikawa M, Adelstein RS. Phosphorylation of phospholamban by calcium-activated, phospholipid-dependent protein kinase. Stimulation of cardiac sarcoplasmic reticulum calcium uptake. *J Biol Chem.* 1984;259(13):8029–8032.
40. Simmerman HK, Collins JH, Theibert JL, Wegener AD, Jones LR. Sequence analysis of phospholamban. *J Biol Chem.* 1986;261(28):13333–13341.
41. Iwasa Y, Hosey MM. Phosphorylation of cardiac sarcolemma proteins by the calcium-activated phospholipid-dependent protein kinase. *J Biol Chem.* 1984;259(1):534–540.
42. Borland G, Bird RJ, Palmer TM, Yarwood SJ. Activation of protein kinase Calpha by EPAC is required for the ERK- and CCAAT/Enhancer-binding protein β-dependent induction of the *SOCS-3* gene by cyclic AMP in COS1 cells. *J Biol Chem.* 2009; 284(26):17391–17403.
43. Braz JC, et al. PKC-α regulates cardiac contractility and propensity toward heart failure. *Nat Med.* 2004; 10(3):248–254.
44. Luo J, et al. A protocol for rapid generation of recombinant adenoviruses using the AdEasy system. *Nat Protoc.* 2007;2(5):1236–1247.
45. Kim S-J, et al. Differential regulation of inotropy and lusitropy in overexpressed Gsα myocytes through cAMP and Ca^{2+} channel pathways. *J Clin Invest.* 1999;103(7):1089–1097.
46. Marx SO, Marks AR. Dysfunctional ryanodine receptors in the heart: new insights into complex cardiovascular diseases. *J Mol Cell Cardiol.* 2013; 58:225–231.
47. Hittinger L, et al. Isoproterenol-induced alterations in myocardial blood flow, systolic and diastolic function in conscious dogs with heart failure. *Circulation.* 1989;80(3):658–668.
48. Sano M, et al. p53-induced inhibition of Hif-1 causes cardiac dysfunction during pressure overload. *Nature.* 2007;446(7134):444–448.
49. Pan Z, et al. MicroRNA-101 inhibited postinfarct cardiac fibrosis and improved left ventricular compliance via the FBJ osteosarcoma oncogene/transforming growth factor-β_1 pathway. *Circulation.* 2012; 126(7):840–850.
50. Kim J, Eckhart AD, Eguchi S, Koch WJ. β-adrenergic receptor-mediated DNA synthesis in cardiac fibroblasts is dependent on transactivation of the epidermal growth factor receptor and subsequent activation of extracellular signal-regulated kinases. *J Biol Chem.* 2002;277(35):32116–32123.
51. Li N, et al. Inhibition of CaMKII phosphorylation of RyR2 prevents induction of atrial fibrillation in FKBP12.6 knockout mice. *Circ Res.* 2012; 110(3):465–470.
52. Temple J, et al. Atrial fibrillation in KCNE1-null mice. *Circ Res.* 2005;97(1):62–69.
53. Chen YJ, et al. Effects of rapid atrial pacing on the arrhythmogenic activity of single cardiomyocytes from pulmonary veins: implication in initiation of atrial fibrillation. *Circulation.* 2001; 104(23):2849–2854.
54. Chen YJ, Chen SA, Chang MS, Lin CI. Arrhythmogenic activity of cardiac muscle in pulmonary veins of the dog: implication for the genesis of atrial fibrillation. *Cardiovasc Res.* 2000;48(2):265–273.
55. Pereira L, et al. The cAMP binding protein Epac modulates Ca^{2+} sparks by a Ca^{2+}/calmodulin kinase signalling pathway in rat cardiac myocytes. *J Physiol.* 2007;583(pt 2):685–694.
56. Chu G, Lester JW, Young KB, Luo W, Zhai J, Kranias EG. A single site (Ser^{16}) phosphorylation in phospholamban is sufficient in mediating its maximal cardiac responses to β-agonists. *J Biol Chem.* 2000; 275(49):38938–38943.
57. Brixius K, Wollmer A, Bolck B, Mehlhorn U, Schwinger RH. Ser^{16}-, but not Thr^{17}-phosphorylation of phospholamban influences frequency-dependent force generation in human myocardium. *Pflugers Arch.* 2003;447(2):150–157.
58. Ling H, et al. Requirement for Ca^{2+}/calmodulin-dependent kinase II in the transition from pressure overload-induced cardiac hypertrophy to heart failure in mice. *J Clin Invest.* 2009;119(5):1230–1240.
59. Engelhardt S, Hein L, Dyachenkow V, Kranias EG, Isenberg G, Lohse MJ. Altered calcium handling is critically involved in the cardiotoxic effects of chronic β-adrenergic stimulation. *Circulation.* 2004; 109(9):1154–1160.
60. He H, et al. Effects of mutant and antisense RNA of phospholamban on SR Ca^{2+}-ATPase activity and cardiac myocyte contractility. *Circulation.* 1999; 100(9):974–980.
61. Eizema K, et al. Adenovirus-based phospholamban antisense expression as a novel approach to improve cardiac contractile dysfunction: comparison of a constitutive viral versus an endothelin-1-responsive cardiac promoter. *Circulation.* 2000; 101(18):2193–2199.
62. Marks AR. Calcium cycling proteins and heart failure: mechanisms and therapeutics. *J Clin Invest.* 2013; 123(1):46–52.
63. Greiser M, Lederer WJ, Schotten U. Alterations of atrial Ca^{2+} handling as cause and consequence of atrial fibrillation. *Cardiovasc Res.* 2011;89(4):722–733.
64. Voigt N, et al. Enhanced sarcoplasmic reticulum Ca^{2+} leak and increased Na^{+}-Ca^{2+} exchanger function underlie delayed afterdepolarizations in patients with chronic atrial fibrillation. *Circulation.* 2012;125(17):2059–2070.
65. Fuster V, et al. ACC/AHA/ESC Guidelines for the Management of Patients With Atrial Fibrillation: Executive Summary A Report of the American College of Cardiology/American Heart Association Task Force on Practice Guidelines and the European Society of Cardiology Committee for Practice Guidelines and Policy Conferences (Committee to Develop Guidelines for the Management of Patients With Atrial Fibrillation) Developed in Collaboration With the North American Society of Pacing and Electrophysiology. *Circulation.* 2001; 104(17):2118–2150.
66. Edes I, Kranias EG. Phospholamban and troponin I are substrates for protein kinase C in vitro but not in intact beating guinea pig hearts. *Circ Res.* 1990; 67(2):394–400.
67. Yamamura K, Steenbergen C, Murphy E. Protein kinase C and preconditioning: role of the sarcoplasmic reticulum. *Am J Physiol Heart Circ Physiol.* 2005;

289(6):H2484–H490.
68. Grimm M, Brown JH. β-adrenergic receptor signaling in the heart: role of CaMKII. *J Mol Cell Cardiol.* 2010;48(2):322–330.
69. Metrich M, et al. Epac mediates beta-adrenergic receptor-induced cardiomyocyte hypertrophy. *Circ Res.* 2008;102(8):959–965.
70. Wang H, et al. Phospholipase C ε modulates β-adrenergic receptor-dependent cardiac contraction and inhibits cardiac hypertrophy. *Circ Res.* 2005; 97(12):1305–1313.
71. Zhang L, et al. Phospholipase Cepsilon hydrolyzes perinuclear phosphatidylinositol 4-phosphate to regulate cardiac hypertrophy. *Cell.* 2013; 153(1):216–227.
72. Klein G, et al. Increased collagen deposition and diastolic dysfunction but preserved myocardial hypertrophy after pressure overload in mice lacking PKCε. *Circ Res.* 2005;96(7):748–755.
73. Doetschman T. Influence of genetic background on genetically engineered mouse phenotypes. *Methods Mol Biol.* 2009;530:423–433.
74. Yoshiki A, Moriwaki K. Mouse phenome research: implications of genetic background. *ILAR J.* 2006; 47(2):94–102.
75. Tang T, et al. Adenylyl cyclase type V deletion increases basal left ventricular function and reduces left ventricular contractile responsiveness to β-adrenergic stimulation. *Basic Res Cardiol.* 2006;101(2):117–126.
76. Tadano M, et al. Congenital semilunar valvulogenesis defect in mice deficient in phospholipase C epsilon. *Mol Cell Biol.* 2005;25(6):2191–2199.
77. Engle SJ, Hoying JB, Boivin GP, Ormsby I, Gartside PS, Doetschman T. Transforming growth factor β1 suppresses nonmetastatic colon cancer at an early stage of tumorigenesis. *Cancer Res.* 1999; 59(14):3379–3386.
78. Engle SJ, et al. Elimination of colon cancer in germ-free transforming growth factor β 1-deficient mice. *Cancer Res.* 2002;62(22):6362–6366.
79. Yagi T, et al. A novel ES cell line, TT2, with high germline-differentiating potency. *Anal Biochem.* 1993; 214(1):70–76.
80. Ishikawa Y, et al. Downregulation of adenylylcyclase types V and VI mRNA levels in pacing-induced heart failure in dogs. *J Clin Invest.* 1994;93(5):2224–2229.
81. Iwatsubo K, et al. Direct inhibition of type 5 adenylyl cyclase prevents myocardial apoptosis without functional deterioration. *J Biol Chem.* 2004; 279(39):40938–40945.
82. Sato M, et al. Activator of G protein signaling 8 (AGS8) is required for hypoxia-induced apoptosis of cardiomyocytes. *J Biol Chem.* 2009; 284(45):31431–31440.
83. Yokoyama U, Patel HH, Lai NC, Aroonsakool N, Roth DM, Insel PA. The cyclic AMP effector Epac integrates pro- and anti-fibrotic signals. *Proc Natl Acad Sci U S A.* 2008;105(17):6386–6391.
84. LaRocca TJ, et al. β2-Adrenergic receptor signaling in the cardiac myocyte is modulated by interactions with CXCR4. *J Cardiovasc Pharmacol.* 2010; 56(5):548–559.
85. Nishimaru K, Kobayashi M, Matsuda T, Tanaka Y, Tanaka H, Shigenobu K. α-Adrenoceptor stimulation-mediated negative inotropism and enhanced Na^+/Ca^{2+} exchange in mouse ventricle. *Am J Physiol Heart Circ Physiol.* 2001;280(1):H132–H141.
86. Adachi-Akahane S, Lu L, Li Z, Frank JS, Philipson KD, Morad M. Calcium signaling in transgenic mice overexpressing cardiac Na+-Ca2+ exchanger. *J Gen Physiol.* 1997;109(6):717–729.
87. Namekata I, et al. Intracellular mechanisms and receptor types for endothelin-1-induced positive and negative inotropy in mouse ventricular myocardium. *Naunyn Schmiedebergs Arch Pharamacol.* 2008; 376(6):385–395.
88. Tanaka H, et al. Unique excitation-contraction characteristics of mouse myocardium as revealed by SEA0400, a specific inhibitor of Na+-Ca2+ exchanger. *Naunyn Schmiedebergs Arch Pharmacol.* 2005;371(6):526–534.
89. Takamatsu H, Nagao T, Ichijo H, Adachi-Akahane S. L-type Ca2+ channels serve as a sensor of the SR Ca2+ for tuning the efficacy of Ca2+-induced Ca2+ release in rat ventricular myocytes. *J Physiol.* 2003; 552(pt 2):415–424.
90. Adachi T, et al. The mechanism of increased postnatal heart rate and sinoatrial node pacemaker activity in mice. *J Physiol Sci.* 2013;63(2):133–146.
91. Adachi-Akahane S, Cleemann L, Morad M. Cross-signaling between L-type Ca^{2+} channels and ryanodine receptors in rat ventricular myocytes. *J Gen Physiol.* 1996;108(5):435–454.
92. Takeshita D, et al. A new calpain inhibitor protects left ventricular dysfunction induced by mild ischemia-reperfusion in in situ rat hearts. *J Physiol Sci.* 2013;63(2):113–123.
93. Namekata I, et al. Involvement of the Na+/Ca2+ exchanger in the automaticity of guinea-pig pulmonary vein myocardium as revealed by SEA0400. *J Pharmacol Sci.* 2009;110(1):111–116.
94. Takahara A, et al. Electrophysiological and pharmacological characteristics of triggered activity elicited in guinea-pig pulmonary vein myocardium. *J Pharmacol Sci.* 2011;115(2):176–181.

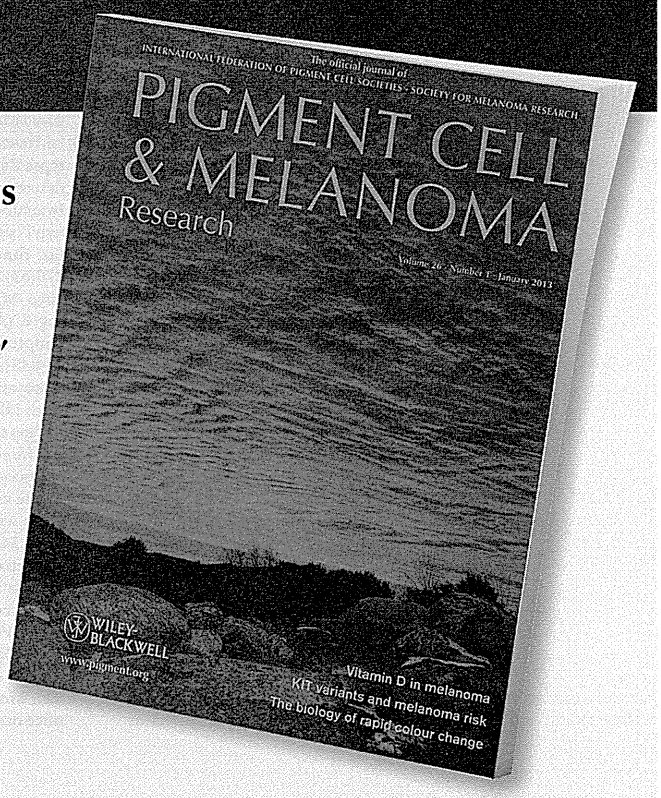

Epac1 increases migration of endothelial cells and melanoma cells via FGF2-mediated paracrine signaling

Erdene Baljinnyam, Masanari Umemura, Christine Chuang, Mariana S. De Lorenzo, Mizuka Iwatsubo, Suzie Chen, James S. Goydos, Yoshihiro Ishikawa, John M. Whitelock and Kousaku Iwatsubo

DOI: 10.1111/pcmr.12250

ORIGINAL ARTICLE

Epac1 increases migration of endothelial cells and melanoma cells via FGF2-mediated paracrine signaling

Erdene Baljinnyam[1], Masanari Umemura[1,2], Christine Chuang[3], Mariana S. De Lorenzo[1], Mizuka Iwatsubo[1], Suzie Chen[4], James S. Goydos[5], Yoshihiro Ishikawa[1,2], John M. Whitelock[6] and Kousaku Iwatsubo[1,2]

1 Department of Cell Biology and Molecular Medicine, New Jersey Medical School-Rutgers, The State University of New Jersey, Newark, NJ, USA **2** Cardiovascular Research Institute, Yokohama City University Graduate School of Medicine, Yokohama, Japan **3** The Heart Research Institute, Newtown, NSW, Australia **4** Susan Lehman Cullman Laboratory for Cancer Research Ernest Mario School of Pharmacy, Rutgers, The State University of New Jersey, Piscataway, NJ, USA **5** The Cancer Institute of New Jersey, New Brunswick, NJ, USA **6** Graduate School of Biomedical Engineering, The University of New South Wales, Kensington, NSW, Australia

CORRESPONDENCE Kousaku Iwatsubo and Erdene Baljinnyam, e-mails: iwatsuko@njms.rutgers.edu; baljiner@njms.rutgers.edu

KEYWORDS Epac/heparan sulfate/human umbilical vein endothelial cells/cell–cell communication/FGF2/migration/angiogenesis/paracrine signaling

PUBLICATION DATA Received 5 April 2013, revised and accepted for publication 9 April 2014, published online 11 April 2014

doi: 10.1111/pcmr.12250

Summary

Fibroblast growth factor (FGF2) regulates endothelial and melanoma cell migration. The binding of FGF2 to its receptor requires N-sulfated heparan sulfate (HS) glycosamine. We have previously reported that Epac1, an exchange protein activated by cAMP, increases N-sulfation of HS in melanoma. Therefore, we examined whether Epac1 regulates FGF2-mediated cell–cell communication. Conditioned medium (CM) of melanoma cells with abundant expression of Epac1 increased migration of human umbilical endothelial cells (HUVEC) and melanoma cells with poor expression of Epac1. CM-induced increase in migration was inhibited by antagonizing FGF2, by the removal of HS and by the knockdown of Epac1. In addition, knockdown of Epac1 suppressed the binding of FGF2 to FGF receptor in HUVEC, and *in vivo* angiogenesis in melanoma. Furthermore, knockdown of Epac1 reduced N-sulfation of HS chains attached to perlecan, a major secreted type of HS proteoglycan that mediates the binding of FGF2 to FGF receptor. These data suggested that Epac1 in melanoma cells regulates melanoma progression via the HS–FGF2-mediated cell–cell communication.

Introduction

Despite recent advances in melanoma therapies utilizing inhibitors of the ERK-signaling pathway, prognosis of advanced melanoma is still poor. In addition, acquired resistance becomes a critical problem with those inhibitors (Little et al., 2012; Maurer et al., 2011). Therefore, the development of a novel therapeutic strategy is an urgent demand for this life-threatening disease. cAMP signaling controls a variety of cellular functions in cancer cells. Exchange protein activated by cAMP (Epac), a guanine nucleotide exchange factor, was found as an additional target of cAMP apart from the conventional one, that is, protein kinase A (De Rooij et al., 1998). Two isoforms of Epac, Epac1 and Epac2, mediate cAMP signaling by the activation of a small-molecular-weight G protein, Rap1 (Bos, 2006). In cancer cells, reports have demonstrated following functions of Epacs such as cell adhesion in human ovarian carcinoma Ovcar3 cells (Quilliam et al., 2002), apoptosis (Tiwari et al., 2004)

Significance

There is an emerging need for elucidating the mechanism of cell–cell interaction in melanoma progression. Our study provides information regarding FGF2-related cell–cell interaction between melanoma/endothelial and melanoma/melanoma cells which is regulated by melanoma cells with the higher expression of Epac1.

and growth arrest (Grandoch et al., 2009a) in B lymphoma cells, formation of embryonic vasculogenic networks in melanoma cells (Lissitzky et al., 2009), and proliferation of prostate carcinoma cells (Grandoch et al., 2009b). We have previously reported that Epac1 is expressed in various melanoma cell lines (Baljinnyam et al., 2011) and plays a role in cell migration via modification of heparan sulfate (HS) glycosaminoglycan (HSPG) chains. The increased migration by Epac1-enhanced metastasis to the lungs in mice (Baljinnyam et al., 2009). Recently, we have also found that, in addition to this HS-related mechanism, a Ca^{2+}-dependent mechanism is also involved in Epac1-induced melanoma cell migration. Epac1 releases cytosolic Ca^{2+} from the endoplasmic reticulum (ER) via the phospholipase C (PLC)/inositol triphosphate (IP3)/IP3 receptor pathway (Baljinnyam et al., 2010). These data suggested that Epac1 plays a critical role in melanoma cell migration via at least two independent mechanisms, that is, the HS-related and the Ca^{2+}-dependent mechanisms.

Fibroblast growth factor-2 (FGF2) is known to increase tumor growth and metastasis by the activation of migration of cancer and vascular endothelial cells (Hibino et al., 2005; Meier et al., 2003; Montesano et al., 1986; Moscatelli et al., 1986; Nugent et al., 2000; Ponta et al., 1998; Sola et al., 1997; Taylor et al., 1993). Binding of FGF2 to FGF receptor requires coordination with N-sulfated glucosamine (Faham et al., 1996; Kreuger et al., 1999; Maccarana et al., 1993; Schlessinger et al., 2000), a component of HS chain (Iozzo and San Antonio, 2001). In addition, perlecan, one of the HSPGs, attaches to FGF2 for its binding to FGF receptors (Knox et al., 2002; Sharma et al., 1998). We have previously reported that, in a human melanoma cell line, Epac1 increases NDST-1, which converts N-acetylated glucosamine into N-sulfated form (Baljinnyam et al., 2009). In addition, it was suggested that Epac1 overexpression increases N-sulfation of HS chain (Baljinnyam et al., 2009).These data led us to examine the hypothesis that Epac1 can control FGF2 signaling by modification of N-sulfation of HS, most probably on perlecan. Further, as secreted FGF2 can act in a paracrine fashion, it is possible that melanoma cells expressing Epac1 regulate migration of surrounding endothelial or other melanoma cells. In this study, we found that Epac1 in melanoma cells increases N-sulfation of secreted perlecan and activates migration of endothelial/melanoma cells by FGF2/HS-mediated cell-cell interaction. In addition, the Epac1 in melanoma cells activates angiogenesis *in vivo*, which may support the survival of other melanoma cells expressing lower amounts of Epac1. Therefore, in addition to our previous reports showing the role of Epac1 in melanoma cells, this study demonstrated that expression of Epac1 in melanoma cells plays a role in melanoma progression by controlling cell/cell communication with endothelial cells and other melanoma cells.

Results

Epac1 in melanoma cells increases migration of neighboring endothelial cells via cell/cell communication

It was suggested that Epac1-expressing melanoma cells can increase migration of neighboring endothelial cells via N-sulfation of HSPG, and subsequently, the activation of paracrine-acting FGF2 signaling. Therefore, we investigated whether melanoma cells with abundant Epac1 expression can increase migration of those with scarce Epac1 expression. According to our previous report (Baljinnyam et al., 2010, 2011), in this study, we have divided the cell lines into two groups: Epac1-rich cell lines, in which Epac1 expression is of the same or higher level than that in SK-Mel-2 (SK-Mel-2, SK-Mel-24, SK-Mel187, and C8161 cells). Epac1-poor cell lines, in which Epac1 expression is lower than a half of Epac1 expression in SK-Mel-2 (HEMA-LP, WM3248, WM1552C, and WM115 cells). Conditioned medium (CM) of C8161 cells, which expresses abundant Epac1 (Baljinnyam et al., 2011), increased migration of human umbilical vein endothelial cells (HUVEC) (Figure 1A). Both a neutralizing antibody against FGF2 and heparitinase, a HS-cleaving enzyme, inhibited the CM-induced HUVEC migration. Knockdown of Epac1 in C8161 cells (Figure 1B) suppressed the CM-induced HUVEC migration (Figure 1A). Hence, these data suggested that Epac1 in melanoma cells can increase migration of endothelial cells via FGF2- and/or HS-dependent mechanisms.

Epac1 in melanoma cells induces tube formation of endothelial cells via cell/cell communication

As endothelial cell migration is fundamental for angiogenesis (Lamalice et al., 2007), we examined whether Epac1-expressing melanoma cells can stimulate endothelial tube formation, which mimics *in vivo* angiogenesis. As shown in Figure 2A, B, CM of C8161 cells increased tube formation of HUVEC. Similar to migration (Figure 1A), the CM-induced tube formation was inhibited by the neutralizing antibody against FGF2 and by heparitinase. In addition, CM of C8161 cells in which Epac1 was knocked down showed reduced tube formation (Figure 2A, B). *In vivo* angiogenesis assay showed the same effect of Epac1 knockdown (Figure 2C, D). These data suggested that Epac1 in melanoma cells have the ability to induce angiogenesis via FGF2- and/or HS-mediated cell/cell communication.

Epac1 in melanoma cells increases migration of neighboring melanoma cells via cell/cell communication

Based on the increased HUVEC cell migration shown previously, we hypothesized that a similar cell/cell interaction may also exist among melanoma cells. To test this hypothesis, we examined whether CM derived from a melanoma cell line affects migration of other melanocyte/

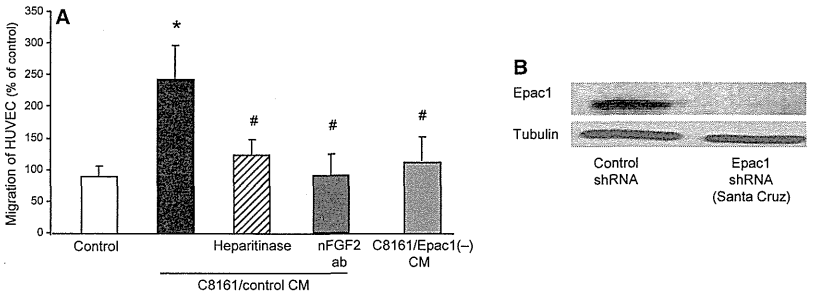

Figure 1. Epac1 in melanoma cells increases migration of endothelial cells via cell/cell communication. (A) CM of C8161 (C8161/control CM) increased migration of human umbilical vein endothelial cells (HUVEC). Epac1 knockdown in C8161 cells (C8161/Epac1(–) CM) inhibited the CM-induced migration. The CM-induced increase in migration was inhibited by the neutralizing antibody against FGF2 [nFGF2 ab (25 μg/ml)], and heparitinase (0.08 U/ml). *P < 0.05 versus control, #P < 0.05 versus C8161/control CM, n = 4. (B) Western blot of C8161 cells with stable knockdown of Epac1 performed with lentivirus-based shRNA induction.

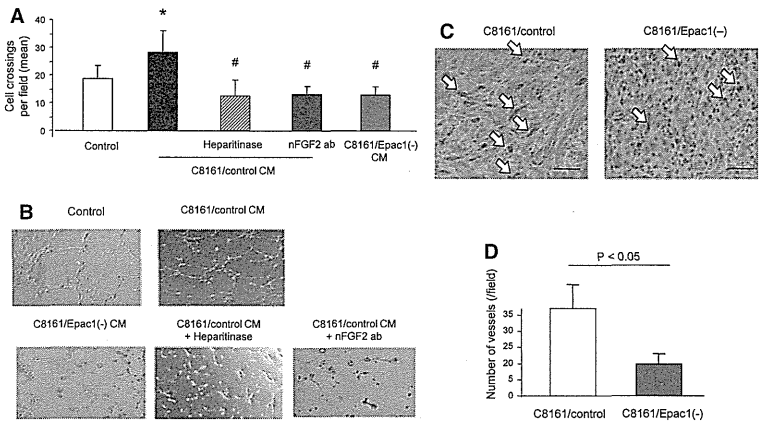

Figure 2. Epac1 in melanoma cells activates angiogenesis. (A) C8161/control CM increased tube formation of human umbilical vein endothelial cells (HUVEC). C8161/Epac1(–) CM showed reduced tube formation compared to C8161/control CM. The C8161/control CM-induced tube formation was inhibited by nFGF2 ab (25 μg/ml), and by heparitinase (0.08 U/ml). C8161/Epac1(–) CM showed reduced tube formation compared with C8161/control CM.*P < 0.01 versus control medium. #P < 0.01 versus C8161/control CM, n = 4. (B) Representative images of HUVEC tube formation described in A. (C and D) Epac1 knockdown reduces angiogenesis *in vivo*. C8161 cells with or without Epac1 knockdown (1 × 10^6 cells) were inoculated in the interscapular region of BALB/c mice. One week after the inoculation, tumor was removed. (C) Immunohistochemical images with anti-CD31 staining for the detection of endothelial cells are shown. White arrows indicate CD31-positive cells stained brown. Scale bar: 100 μm. (D) The number of microvessels in each mouse was counted with the positively stained cells in 10 different fields, n = 4.

melanoma cells. CM from WM3248 or WM115 cells, both primary melanoma cell lines, did not change cell migration of HEMA-LP melanocyte cells (Figure 3A). In contrast, CM sourced from SK-Mel-2 or C8161 cells, both metastatic melanoma cell lines, increased migration of HEMA-LP. Migration of WM1552C cells, a primary melanoma cell line of the radial growth phase (RGP), was examined next (Figure 3B). CM of WM3248, a melanoma cell line of the vertical growth phase (VGP), SK-Mel-187, SK-Mel-2, or C8161 cells, all metastatic melanoma cell lines, increased WM1552C cell migration (Figure S3). In contrast, migration of the metastatic melanoma cell line, C8161 cells, was not affected by CM of SK-Mel-2. Epac1 overexpression (OE) in Epac1-poor melanoma cells indeed increased cell migration in both WM115 and WM3248 cells (Figure S1), suggesting that Epac1's effect on migration is saturated in Epac1-rich melanoma cells such as C8161 and SK-Mel-2 cells. Epac1 knockdown by two different Epac1 shRNAs (from Santa Cruz Biotechnology and Sigma Aldrich) in C8161 cells inhibited the CM-induced migration of HEMA-LP and WM1552C cells (Figure 3A, B and S2). Similar result was obtained in Epac1 knockdown in SK-Mel-2 cells (Figure 3B). These data suggested the specific role of Epac1 in the CM-induced migration.

The CM-induced migration of HEMA-LP and WM1552C cells were inhibited by heparitinase (Figure 3A and B), and the CM-induced migration of WM1552C cells was suppressed by the neutralizing FGF2 antibody (Figure 3B). The neutralizing FGF2 antibody inhibited CM-induced migration in other combinations of CM and cell lines used for migration (Figure S3). In addition, Epac1 OE in WM3248 cells increased their migration, and it was reduced by neutralizing FGF2 antibody (Figure S4).These

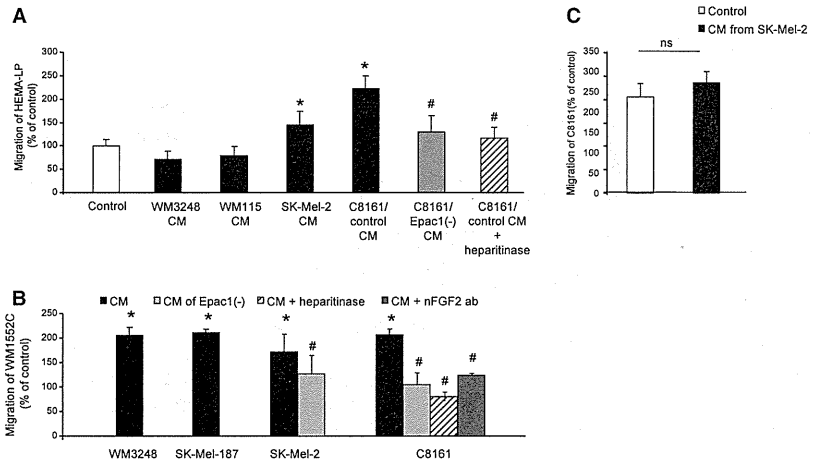

Figure 3. Epac1 in melanoma cells increases migration of melanocytes/other melanoma cells. (A) Conditioned media of indicated melanoma cell lines were used for the Boyden chamber migration assay of HEMA-LP cells. Conditioned media from SK-Mel-2 and C8161 cells, but not those from WM3248 and WM115 cells, increased migration of HEMA-LP cells. Knockdown of Epac1 (C8161/Epac1(−) CM) as well as heparitinase inhibited the CM-induced migration. *P < 0.05 versus control medium, #P < 0.05 versus C8161/control CM, n = 4. (B) Conditioned media of indicated melanoma cell lines were used for the Boyden chamber assay of WM1552C cells. Conditioned media of all cell lines examined increased migration of WM1552C cells. Knockdown of Epac1 inhibited migration induced by CM derived from SK-Mel-2 and C8161 cells. Heparitinase and the nFGF-2 antibody suppressed migration induced by CM of C8161 cells.*P < 0.05 versus control medium, #P < 0.05 versus CM, n = 4. (C) The Boyden chamber assay showed that CM of SK-Mel-2 cells did not increase migration of C8161 cells, n = 4.

data suggested that CM-induced migration was regulated by Epac1, HS and/or FGF2 signaling.

Epac1 augments the binding of FGF2 to FGF receptor

We next investigated the effects of Epac1 on HS including N-sulfation and FGF2 signaling. It has been demonstrated that perlecan interacts with FGF2 via its HS chains (Knox et al., 2002; Sharma et al., 1998). We thus examined perlecan expression of CM by isolation with chromatography. N-sulfated HS chains of perlecan were detected by the anti-HS antibody (clone 10E4) (Figure 4A). The N-sulfation of HS bound to the perlecan was significantly reduced by Epac1 knockdown. In addition, both the amount of N-sulfation and the number of FGF receptors bound to FGF2 were decreased by knockdown of Epac1 (Figure 4B). In contrast, neither the expression of total HS bound to FGF2 nor FGF2 itself in CM were changed by Epac1 knockdown (Figure 4B), suggesting that Epac1 enhances FGF2-binding to FGF receptor via N-sulfation of HS. The binding assay showed that CM from C8161 cells increases FGF2 binding to FGF receptor expressed in HUVEC cells. The CM-induced FGF2 binding was inhibited by the FGF2 antibody and by Epac1 knockdown in C8161 cells (Figure 4C). Taken together, these data demonstrated that Epac1-expressing melanoma cells regulate paracrine-acting FGF2 signaling in neighboring cells such as endothelial and melanoma cells by modification of HS.

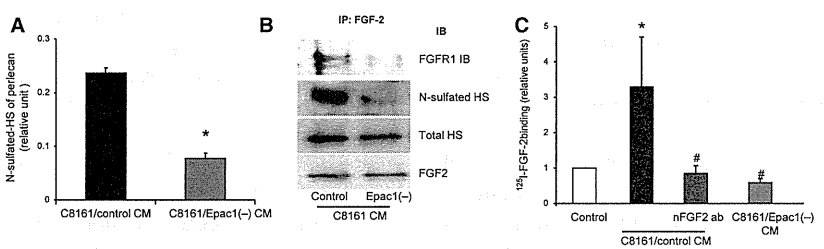

Figure 4. Epac1 enhances the binding of fibroblast growth factor (FGF2) to FGF receptor via N-sulfation of HS. (A) Perlecan was isolated from the DEAE chromatography fractions using a polyclonal antiperlecan antibody. The presence of HS chains on perlecan was detected using an anti-HS-specific antibody (10E4). Epac1 knockdown reduced the amount of N-sulfated HS attached to perlecan. *P < 0.05 versus C8161/control CM, n = 8. (B) CM of C8161 was subjected to immunoprecipitation with the antibody against FGF2 followed by Western blot for indicated antibodies. Both N-sulfated HS and FGF receptor 1 (FGFR1) attached to FGF2 were reduced by Epac1 knockdown whereas the amount of FGF2 in the CM was not different. (C) The binding assay for FGF2 in human umbilical vein endothelial cells (HUVEC) was performed with indicated CM. C8161/control CM increased the binding of FGF2 to HUVEC. The neutralizing antibody for FGF2 (nFGF2 ab) and knockdown of Epac1 inhibited the CM-induced FGF2 binding. *P < 0.05 versus control medium, #P < 0.05 versus C8161/control CM, n = 4.

Epac1-rich melanoma cells support proliferation of Epac1-poor melanoma cells *in vivo*

Increased angiogenesis by Epac1 (Figure 2) suggested that Epac1-rich melanoma cells can support proliferation not only of Epac1-rich melanoma cells themselves but also of Epac1-poor melanoma cells via newly supplied blood flow. If this is the case, melanoma cells expressing low Epac1 that cannot survive *in vivo* are rescued by coexistence of Epac1-rich melanoma cells. Therefore, we examined whether coinoculation of melanoma cells with high Epac1 expression and those with low Epac1 expression enables the second type of cells to survive in mice. To show this, we used SK-Mel-2 cells, which abundantly express Epac1, and WM1552C cells, which poorly express Epac1 (Baljinnyam et al., 2011). In addition, we used green fluorescent protein (GFP) – or red fluorescent protein (RFP) to distinguish WM1552C cells from SK-Mel-2 cells. Our study showed that SK-Mel-2 cells inoculated in athymic nude mice, but not WM1552C cells, formed a tumor (Figure 5A), suggesting that WM1552C cells alone cannot survive in mice. A tumor was formed by WM1552C cells coinoculated with SK-Mel-2 cells, but not with WM1552C cells inoculated alone (Figure 5A–C). The tumor formed by the coinoculation showed both GFP- and RFP-fluorescent signal (Figure 5D). In addition, fluorescence-activated cell sorting (FACS) analysis demonstrated that individual cells isolated from the tumor have either RFP signal or GFP signal (Table 1). These data showed the existence of both WM1552C and SK-Mel-2 cells in the tumor and thus suggested that Epac1-rich melanoma cells can support the survival of Epac1-poor melanoma cells. As the percentages of GFP- and RFP-positive cells are not equal even in the same SK-Mel-2 cells (Table 1) under *in vivo* conditions, it seems that one of the two inoculated cell lines becomes dominant. As CM of SK-Mel-2 cells did not increase proliferation of WM1552C cells (data not shown), these data suggest that SK-Mel-2 cells enable WM-1552C to survive *in vivo* most probably by modification of the extracellular matrix and enhanced angiogenesis.

Discussion

Our previous reports showed that Epac1 increases migration of melanoma cells themselves (Baljinnyam et al., 2009, 2010, 2011). Epac1 in melanoma cells may regulate the cell–cell communication, which could lead to an augmented migration of neighboring endothelial and melanoma cells. Our findings suggest that Epac1-rich melanoma cells play a major role in melanoma progression through migration of the Epac1-rich melanoma cells themselves, but also through increasing migration of neighboring Epac1-poor melanoma cells and more importantly, by the increased migration of neighboring endothelial cells that can accelerate tumor growth via angiogenesis. Therefore, it is plausible that Epac1-rich population in the melanoma tumor critically regulates tumor growth rate.

Although a number of reports demonstrated the role of FGF2 in melanoma progression (Gartside et al., 2009; Hibino et al., 2005; Meier et al., 2000; Ozen et al., 2004), little attention was focused on the role of paracrine-acting FGF2. Using B16F10, an invasive mouse melanoma cell line, CM-activated capillary formation of bovine aortic endothelial cells (Garrido et al., 1995). CM from A375, a

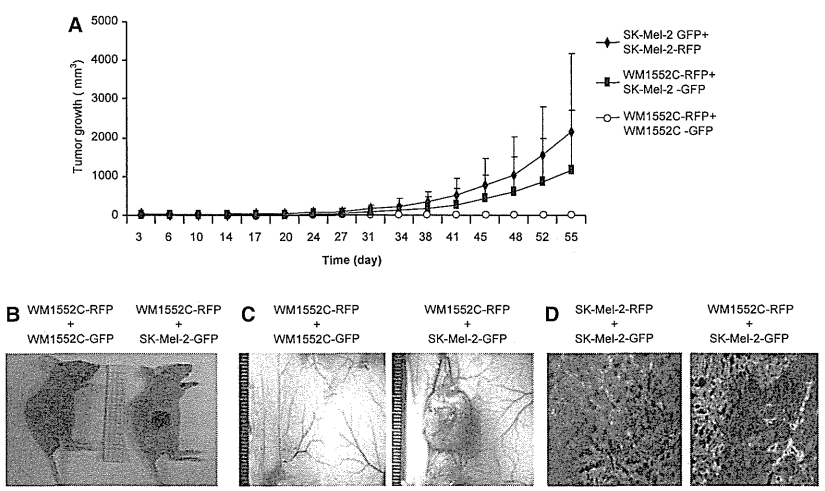

Figure 5. Epac1-rich melanoma cells support survival of Epac1-poor melanoma cells. (A) Tumor growth of WM1552C and SK-Mel-2 cells expressing Red Fluorescent Protein (RFP) and Green Fluorescent Protein (GFP) is shown. A mixture of indicated cells was injected in the right dorsolateral flank region in athymic BALB/c nude mice. Tumor size was measured twice a week to calculate tumor volume. Tumor failed to grow in the mixture of RFP- and GFP-labeled WM1552C. (B and C) Representative images of the tumors in the 12 weeks after the inoculation are shown. The mixture of RFP-labeled WM1552C cells and GFP-labeled SK-Mel-2 cells formed a tumor. (D) Representative images of coimmunostaining for RFP and GFP of the tumors formed by the indicated cell mixtures. Blue indicates 6-diamidino-2-phenylindole (DAPI) staining.

